AD

RESEARCH AND DEVELOPMENT TECHNICAL REPORT

FA-TR-76065

Experimental Pulsed Laser Remote Crosswind Measurement System — Feasibility Study and Design (Part IV)

November 1976

by

J. Fred Holmes
J. Richard Kerr
Myung H. Lee
Michael E. Fossey

Department of Applied Physics & Electronic Science
The Oregon Graduate Center
19600 N.W. Walker Road
Beaverton, Oregon 97005

U.S. ARMY ARMAMENT COMMAND
FRANKFORD ARSENAL
PHILADELPHIA, PENNSYLVANIA 19137

NOTICES

Disclaimers

The findings in this report are not to be construed as an official Department of the Army position, unless so designated by other authorized documents.

The citation of trade names and names of manufacturers in this report is not to be construed as official Government indorsement or approval of commercial products or services referenced herein.

Disposition

Destroy this report when it is no longer needed. Do not return it to the originator.

Unclassified

SECURITY CLASSIFICATION OF THIS PAGE *(When Data Entered)*

REPORT DOCUMENTATION PAGE

READ INSTRUCTIONS BEFORE COMPLETING FORM

1. REPORT NUMBER: FA-TR-76065	2. GOVT ACCESSION NO.
3. RECIPIENT'S CATALOG NUMBER: Rept.	
4. TITLE (and Subtitle): Experimental Pulsed Laser Remote Crosswind Measurement System - Feasibility Study and Design, (Part IV)	5. TYPE OF REPORT & PERIOD COVERED: Interim 15 Oct 1975 - 14 Nov 1976
	6. PERFORMING ORG. REPORT NUMBER
7. AUTHOR(s): J. Fred Holmes, J. Richard Kerr, Myung H. Lee, Michael E. Fossey	8. CONTRACT OR GRANT NUMBER(s): DAAA25-76-C0132 new
9. PERFORMING ORGANIZATION NAME AND ADDRESS: The Oregon Graduate Center, 19600 N.W. Walker Road, Beaverton, Oregon 97005	10. PROGRAM ELEMENT, PROJECT, TASK AREA & WORK UNIT NUMBERS
11. CONTROLLING OFFICE NAME AND ADDRESS: U.S. Army Armament Command, Frankford Arsenal, Philadelphia, Pennsylvania 19137	12. REPORT DATE: 14 Nov 1976
	13. NUMBER OF PAGES: 70
14. MONITORING AGENCY NAME & ADDRESS *(if different from Controlling Office)*: 75p.	15. SECURITY CLASS. *(of this report)*: Unclassified
	15a. DECLASSIFICATION/DOWNGRADING SCHEDULE

16. DISTRIBUTION STATEMENT *(of this Report)*

Approved for public release; distribution unlimited

DAAA25-76-C-0132

17. DISTRIBUTION STATEMENT *(of the abstract entered in Block 20, if different from Report)*

18. SUPPLEMENTARY NOTES

19. KEY WORDS *(Continue on reverse side if necessary and identify by block number)*

Remote Crosswind Measurement, Remote Sensing, Laser Anemometer, Atmospheric Turbulence, Speckle

20. ABSTRACT *(Continue on reverse side if necessary and identify by block number)*

Recent activity with regard to development of a pulsed laser, remote crosswind measurement system is described. This includes a more complete theoretical formulation which includes the log-amplitude perturbation. In addition, cw experimental work used to verify the theoretical formulation and the design and construction of a new pulsed crosswind system are described. The system uses a double pulsed 1.06 μm Nd:YAG laser, a sixteen element arrayed receiver and space-time statistical averaging.

MICRON

DD FORM 1 JAN 73 1473 EDITION OF 1 NOV 65 IS OBSOLETE

407 883

Unclassified

SECURITY CLASSIFICATION OF THIS PAGE *(When Data Entered)*

Experimental Pulsed Laser, Remote Crosswind Measurement System -- Feasibility Study and Design (Part IV)

J. Fred Holmes
J. Richard Kerr
Myung H. Lee
Michael E. Fossey

Contractor: The Oregon Graduate Center

Sponsor: U.S. Army Armament Command
Frankford Arsenal
Philadelphia, Pennsylvania 19137

Contract Number: DAAA25-76-C0132

Effective Date of Contract: 15 October, 1975

Contract Expiration Date: 14 November 1976

Amount of Contract: $98,455

Principal Investigators: Dr. J. Fred Holmes
Dr. J. Richard Kerr

Project Monitors: Mr. Ira I. Goldberg, Frankford Arsenal
Dr. Donald L. Walters, U.S. Army Electronics Command

CONTENTS

SUMMARY

A pulsed laser, remote crosswind measurement system is being developed for remotely sensing the crosswind in the atmosphere by analyzing the laser energy scattered from a diffuse target. The system consists of a 100 millijoule, double-pulse Nd:YAG laser, a sixteen element, pulsed optical receiver and a processor. In order to estimate the crosswind, the variance, covariance and slope of the time delayed covariance function for the received intensity must be measured. This has been accomplished by utilizing an optical receiver array and a combination of space and time averaging to estimate the statistical quantities. Design and construction of the crosswind measurement system has been completed and it will be tested and optimized during the next contract period.

Theoretical formulations for the statistics of the received intensity are needed for system design, optimization and calibration. During the period covered by this report, formulations were developed which include the effects of the log-amplitude covariance as well as the wave structure function and represent a significant extension of previous work. In addition, a major analytical breakthrough was made in our effort to reduce the theoretical formulations to numbers for comparison with experimental results, design and calibration. The theoretical formulations are being verified in a cw field experiment and the results thus far have yielded excellent agreement with this theory.

I. INTRODUCTION AND BACKGROUND

In FY74 Frankford Arsenal through the Atmospheric Sciences Laboratory (ECOM) White Sands Missile Range, New Mexico, initiated a program to develop a remote crosswind measurement system for ballistic applications. A remote crosswind system is needed that will measure the average crosswind between gun and target and automatically feed this data to an onboard ballistics computer for fire control correction of the crosswind error. This error is quite significant, representing one of the largest remaining sources of combat vehicle fire control error, especially with medium and slow muzzle velocity ammunitions.[1]

The feasibility of remotely determining the transverse wind velocity with a point-to-point, cw laser system is well established.[2,3,4] In more recent work,[5-11] investigators have considered the extension of the technique to the use of multiple cw lasers and folded paths as well as ambient light and the use of techniques to overcome saturation. The technique basically consists of relating the scintillation pattern on the receiver, to the frozen-in, transverse motion of the turbulence structure along the propagation path. The most successful cw method that has been used involves the measurement of the slope of the log amplitude covariance function at zero time delay.[2]

Using active cw sources, an acceptable signal to noise ratio can be achieved at reasonable transmitter power levels. However, the proposed application of the work sponsored under this project requires a single-ended system operating against a non-cooperative target which can be viewed as a perfectly diffuse surface with reflectivity of approximately 0.1.[12] Under this constraint, an active cw system would require excessive transmitter power levels.

The primary noise sources in the system are the Poisson fluctuations of detector current and thermal noise in the electronics. For a given pulse energy, as the pulse width decreases the instantaneous power increases. Consequently, the detector signal current increases and eventually its Poisson fluctuation becomes the dominant noise source. If the receiver is gated synchronously with the transmitted pulses, then it would be signal shot noise limited. Therefore, in a direct detection optical system, the signal to noise ratio for a given total energy increases as the pulse duration is made shorter.[13] Consequently, a pulsed system can be made considerably more sensitive than a cw system.

In order to employ a pulsed laser and still make a temporal measurement as required for wind velocity, a double-pulse technique has been used[14,15,16] whereby two Q-switched laser pulses are generated at a time interval on the order of a millisecond. This interval appears to be appropriate for the employment of the covariance "slope at zero time lag" technique[2] and is compatible with current double-pulse laser technology. Initially, a ruby laser was used as a pulsed source.

Since the pulse technique utilizing a ruby laser precluded time averaging of the statistical quantities measured, spatial averaging had to be employed. Therefore the equivalent of an array of detectors was used in order to generate a sufficient number of samples of the instantaneous scintillation pattern to use spatial averaging. To the extent that the statistics of this pattern are invariant with lateral translation at the receiver (a safe assumption with the use of a diffuse target as a secondary source), such spatial averaging will give the desired result, and the pulsed technique is fundamentally similar to the cw, time-averaging approach.

Initially the work on the pulsed laser, remote cross-wind measurement system was based on a technique and theory developed for a cw system utilizing a laser directly as a source. This technique and theory, which is based on log-amplitude statistics, has been verified experimentally and is valid for the cw configuration. The basic cw technique is applicable to the pulsed system. However, the detailed theory does not apply to the pulsed configuration. This is not the result of a difference in the propagation characteristics between the pulsed and cw sources. It is caused by the physical differences in the two systems.

The source for the pulsed system is a laser illuminated, incoherent target yielding a source with an undefined size which at least close to the target gives rise to a temporally coherent, spatially incoherent, Rayleigh distributed field amplitude. This is in contrast to the point source used in the earlier active cw systems and the temporally incoherent cw sources used in later active and passive systems which give rise to log-normal amplitude statistics.

Consequently, the experimental work with the ruby system was concentrated largely on tests where the size of the source (at the target) could be controlled.[16] This allowed a better comparison with available theory by decoupling from the experiment the effects of the atmosphere on the laser beam as it propagates from the transmitter to the target. The controlled source size was accomplished by utilizing small disks of scotch-lite on a black background as a target.

The results of these tests indicated the need both for a better pulsed source and a theory applicable to the pulsed system.

A ruby laser was originally chosen as a source because of cost considerations and the realization that energy levels of the order of a joule or greater might be required. Subsequent analysis and experimental results indicated that energy levels of the order of 100 millijoules would yield an adequate signal to noise ratio in the system. Consequently, the system was redesigned to utilize a Nd:YAG laser operating at 1.06 microns. It has the following advantages over the ruby system: much smaller; more rugged; less sensitive to temperature changes; lighter; less power required; much less RFI; convection cooled; space-time averaging possible.

Most of the advantages of the Nd:YAG system accrue from the much lower threshold of the lasing medium. Consequently it requires a much lower input energy per pulse (on the order of 10 in lieu of 1,000 joules). This allows the YAG laser to be double pulsed at a much higher rate than the ruby laser and makes space-time averaging possible. In addition, the lower input energy greatly reduces radio frequency interference (RFI) between the laser and the receiver.

The use of space-time averaging allowed the size of the optical receiver array (spatial averaging) to be reduced from 64 elements (8 x 8) to 16 elements (2 x 8). The laser can produce a double pulse once every 100 milliseconds and the number of double pulses used for a crosswind measurement can be adjusted from one to forty. Ten double pulses will normally be used for the time averaging which requires about one second. This yields 160 samples per measurement for the YAG system as compared to 64 samples with the old ruby system. An additional advantage of the time averaging is that it will tend to eliminate any intermittency of turbulence problems. The YAG system has been constructed and will be evaluated during the next contract period.

Since a theory applicable to the pulsed system was not available, a new theoretical formulation for the statistics of the received intensity based on the extended Huygens-Fresnel principle was developed.[16,17] This first theoretical effort invoked the assumption of Gaussian field statistics at the receiver. Because of this assumption, only phase perturbation effects, which show up as a dependence on the transverse correlation scale (ρ_o) appear in the result. This was initially thought to be a good assumption, at least for low turbulence levels, on the basis that the relation between the two turbulence scale sizes (ρ_o and $\sqrt{L/k}$) was expected to be multiplicative and therefore the smaller scale - which is usually ρ_o in the present application - would be dominant. This approach has the advantage of yielding a simple theory, but the disadvantage of requiring a receiver to operate over several decades of scale size with the scale size being an exponential function of both target range and turbulence level.

Our cw experiments have confirmed that at low turbulence levels, the Gaussian assumption is indeed correct for the variance and covariance. However at intermediate turbulence levels the scale size approaches $\sqrt{L/k}$. This suggests that the log-amplitude term, which is responsible for this scale size, plays an important part in the statistics of the received intensity and particularly with regard to remote wind sensing.

Consequently, a complete theoretical formulation including the log-amplitude term has been developed. It shows that the relationship between the two scale sizes is additive rather than multiplicative as indicated by the cw experimental data. This means that $\sqrt{L/k}$ scale size is dominant for our application and that the same mechanism which has been used as

a basis for the successful cw wind sensing work performed by NOAA is available for utilization by the pulsed, diffuse-target case. This had not been clear heretofore.

In addition, we achieved a major analytical breakthrough which greatly simplified the formulations while retaining a complete description of the mechanisms involved. We are now able to reduce the formulations to numbers for comparison with the cw experimental results and for design purposes.

These results have very positive implications with regard to the design of a pulsed remote wind sensing system.

II. 1.06 SYSTEM

During the period of this report a system was designed and constructed to remotely sense the crosswind by utilizing a double pulsed neodymium YAG laser as a transmitter. The system was designed to take advantage of the relatively rapid repetition rate possible with the Nd:YAG laser by incorporating temporal averaging in addition to the spatial averaging used with the ruby system[15,16] to obtain more accurate estimates of the statistics of the received intensity.

The overall system is illustrated in Figure II-1. It consists of a double pulsed Nd:YAG laser, a processor for control and data reduction, a sixteen element optical receiver, a four channel analog to digital converter with display, a video display, a wind and range display, a high speed paper tape punch, a teletype and a control panel.

In order to measure the crosswind, the time delayed statistics of the received intensity must be measured. Consequently, a double pulse laser must be used as a source.[14] The laser used in the system was manufactured by International Laser Systems and is basically their model NT-170 modified for double pulse operation. The specifications for the laser are shown in Table II-1 and the laser is shown in Figure II-2.

The overall system control and data processing necessary to carry out the time averaging and perform on site wind calculation was accomplished by using a Computer Automation LSI-2 minicomputer. Interface circuitry and software was developed to allow the minicomputer to control not only the laser and receiver, but also a four channel analog to digital converter and the various input and output devices shown in Figure II-1.

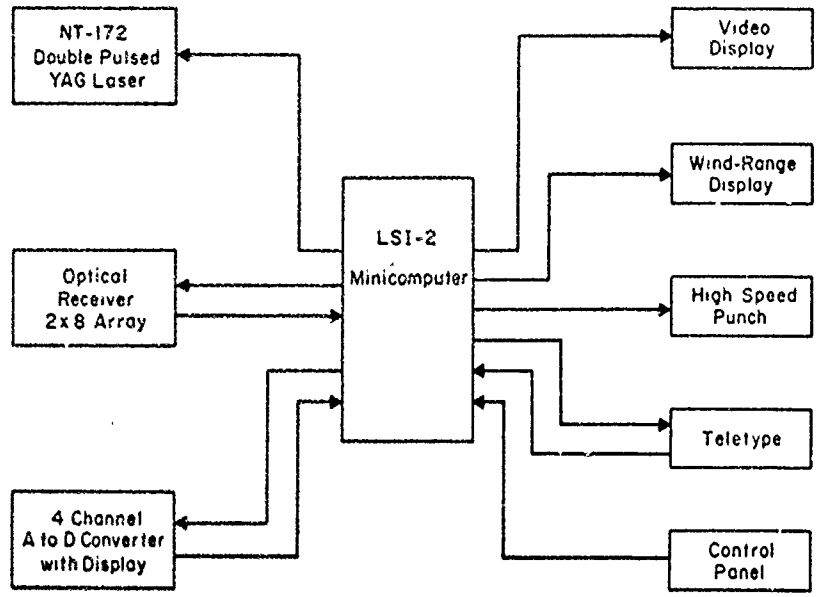

Figure II-1. Pulsed Laser Anemometer System Design

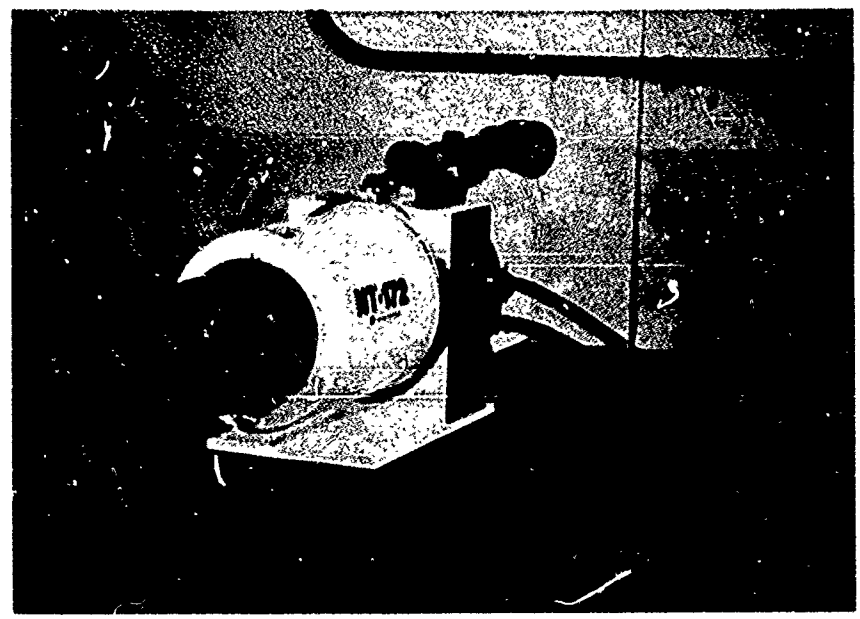

Figure II-2. 1.06 μm Laser

Table II-1. Specifications for Model NT-172
Double-Pulse Laser System

Transmitter:	
Output Wavelength	1.064 μm
Output Beam Divergence	0.3 mr
Beam Diameter	3.0 in.
Energy per Pulse	100 mJ
Pulsewidth	18 nsec, nominal
Repetition Rates	Single-shot, 1, 5 and 10 pps
Double-Pulse Separation	1 millisecond (adjustable)
Operating Temperature	32° to 120°F
Input Power Requirement	24 V dc at 60 A peak, 40 A average
Size	9 x 11 x 25 in.
Weight	43 lb.
Power Supply:	
Input Power Requirement	24 V dc
Size	9 x 11 x 20 in.
Weight	38 lb.
Line Converter:	
Input Power Requirement	115 V, 50 to 60 Hz, 1Ø
Output Power	24 V dc
Size	9 x 11 x 20 in.
Weight	70 lb.

An operating system with the capability to link assembly level control programs to Fortran programs was used to develop the operating software. This combination of machine language and higher level language allows the control and data processing to be very flexible. Scientific computations are carried out by Fortran subroutines which can be written, modified, and debugged much more readily than equivalent assembly language programs. The processor, wind and range displays, and control panel are all housed in a common cabinet as shown in Figure II-3.

The analog to digital converter is designed to be used with propeller anemometers and a Cambell Scientific CA-9 space averaging anemometer to provide in situ wind and turbulence strength data. This allows the in situ data to be recorded under control of the processor for comparison to measurements made with the 1.06 system.

Electronically, the 1.06 system receiver is quite similar to the ruby system.[15] However, the optical and detection portions of the 1.06 system receiver are quite different from that of the ruby system.

The heart of the receiver is a hybrid array of PIN silicon photodiodes. The array consists of 16 one millimeter diameter devices arranged in two horizontal rows. The 8 diodes in each row are mounted on 1.75 mm centers. As shown in Figure II-4, a two lense optical system is used. It is basically a beam reducer that allows the characteristic scale sizes of the turbulence to be reduced to match the detectors. The second lense is easily changed and provides a means of adjusting the magnification and hence the effective array spacing.

Results from the cw experiments indicate that an array spacing around $0.5\sqrt{L/k}$ may be optimum. For the initial experiments

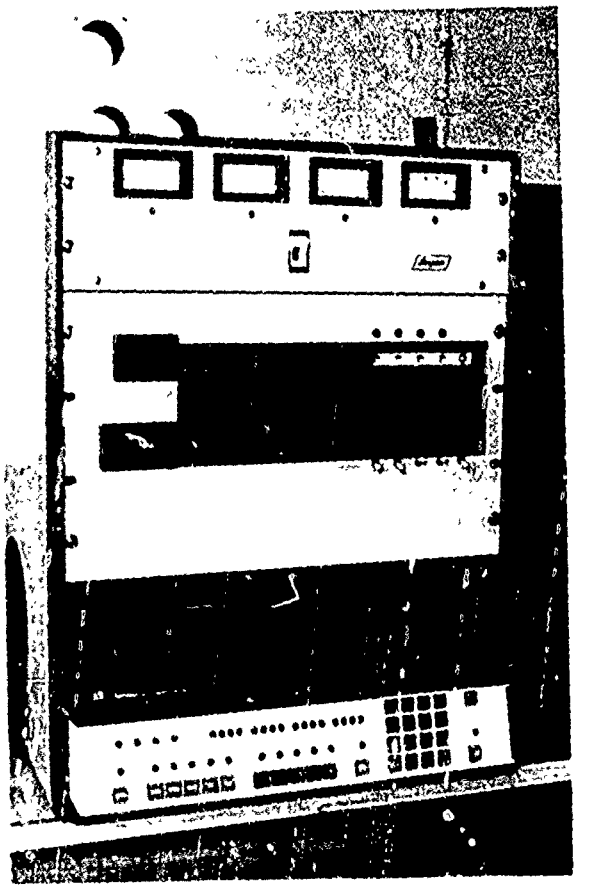

Figure II-3 Processor and Control Panel

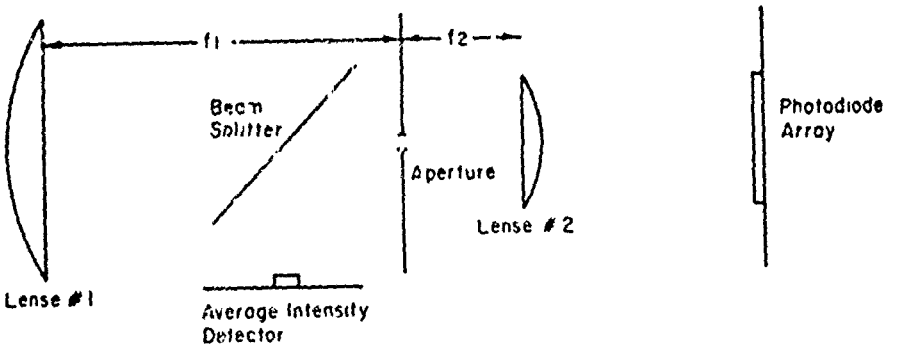

Figure II-4 Receiver Optical Design

at 2000 m ($\sqrt{L/k}$ = 18.4 mm) a 60 mm focal length second lense will be used. In conjunction with the 330 mm objective lense this produces a demagnification of 5.5, an effective detector spacing of 9.625 mm and an effective detector aperture size of 5.5 mm. If future experimental results indicate that adjustment of the effective detector spacing as a function of range is necessary to achieve the desired accuracy over the full operating range, then the beam reducer could be replaced with zoom optics that are automatically adjusted by the computer based on the measured range to the target.

As shown in Figure II-4, a field of view limiting aperture is mounted at the focal point of the objective lense. This serves to limit the amount of background light incident on the detectors. An aperture of 1.6 mm was chosen to limit the field of view to 5 milliradians.

Provision has been made for mounting a removable beam splitter as shown in Figure II-4. It is a piece of uncoated crown glass at a 45° angle to the optical axis and is designed to divert about 9% of the light to a mean intensity detector. A mean intensity detector would provide a more accurate estimate of the mean intensity than can be obtained from averaging the 16 optical channels since the energy is averaged over the entire objective aperture. The beam splitter and mean intensity detector will be added if it proves necessary.

A block diagram of the receiver electronics is shown in Figure II-5. The operation of the signal processing electronics is controlled by a central controller inside the receiver. The operational sequence is initiated by external stimulus but

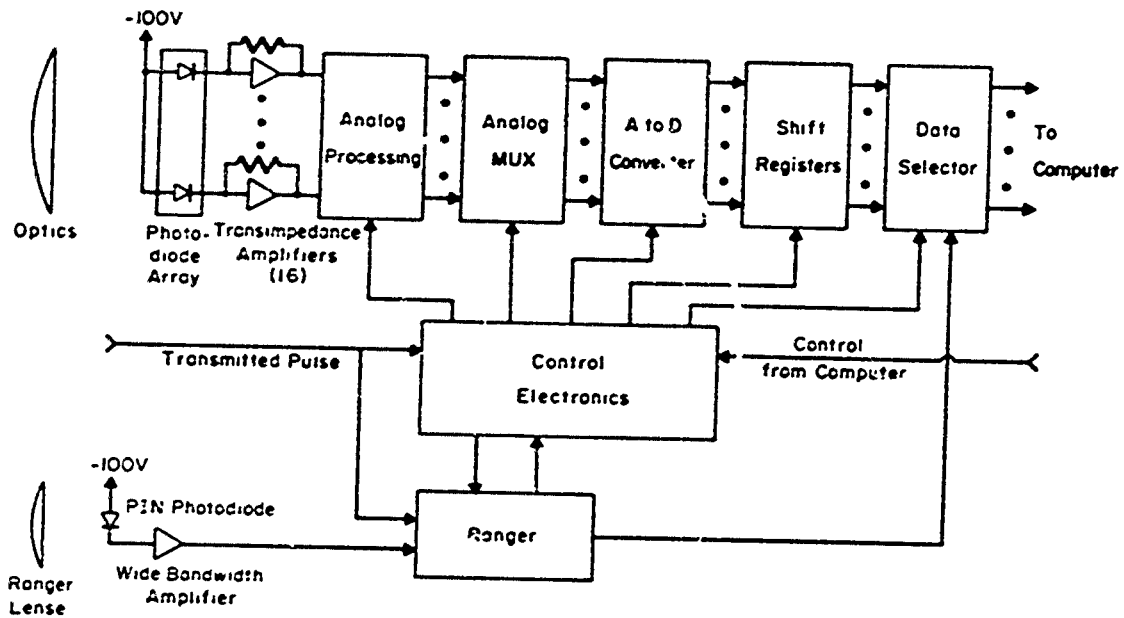

Figure II-5. Receiver Electronics Design

takes place under internal control.

The received signal is detected by the PIN photodiodes and converted from current to voltage by the transimpedance amplifiers. The analog processing circuitry for each channel consists of a variable gain amplifier, an integrator and a sample and hold unit. DC voltages from the sample and hold are converted to digital signals by a 16 channel multiplexed 12 bit A to D converter. This digital information is stored in shift registers that can be accessed by the computer.

An operation cycle is initiated when the computer sends out a control signal requesting DC offset data from the receiver. The integrators are gated open for a precise amount of time and the resulting voltage is converted and stored. The computer then reads this information before firing the laser.

After the laser is fired, the outgoing pulse is detected by a photodiode external to the receiver. A signal from this detector initiates a timing sequence in the control electronics, and starts the counters in the ranger. After a precise interval based on the previous range reading the integrators are gated open to capture the returning pulse and the data is gated and stored. The returning pulse is detected by the ranger detector, and completes the time of flight measurement that indicates range.

One millisecond (this time delay is adjustable) after the first pulse, the second pulse is transmitted, and the process repeats itself, except that the ranger does not operate.

After the information from both pulses is stored, it is transferred to the computer where the data is processed to obtain variance, covariance, time delayed covariance and crosswind.

The signal to noise ratio for the receiver was evaluated using the techniques described in an earlier report.[15] Our calculation yielded a signal to noise ratio of 31 db with a 0.1 reflectivity target at 3 km range and a receiver gate time of 3 microseconds. The lower laser energy (100 millijoules) and smaller detector aperture in the 1.06 system were partially offset by using better amplifiers (wider bandwidth and lower voltage noise) and by operating the photodiodes fully depleted for minimum capacitance.

The ranger has a resolution of 2 meters and a calculated root mean square error of ± 2 meters with an 0.1 reflectivity target at 3 km. The receiver is shown in Figures II-6 through II-9.

Two modes of operation are designed with the control software. When the system is powered up, the operator selects the number of double pulse cycles (limited to less than 41) that are to be used for one sample. This preselected number of cycles is used regardless of the mode of operation selected. In the normal mode, the system is automatically cycled the preset number of times and the measured wind and range are displayed. Then at the operator's option a hard copy of the results and/or a paper tape of the results or raw data may be obtained. In addition, a video display of the raw data is provided to aid the operator in aligning the system and verifying proper operation.

In the cw mode of operation, at the end of the preset number of cycles, the results are punched on paper tape and then the system is automatically cycled again. This continues until the operator terminates the cw mode.

The gain of the system must be adjusted to take into account the decrease in received signal strength with increasing

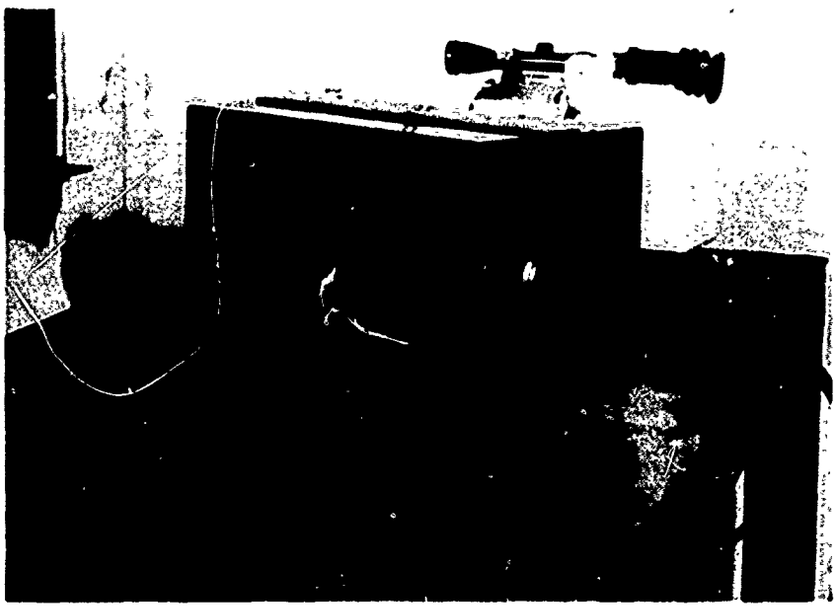

Figure II-6. Receiver

Figure II-7. Receiver, Right Side, Cover Removed

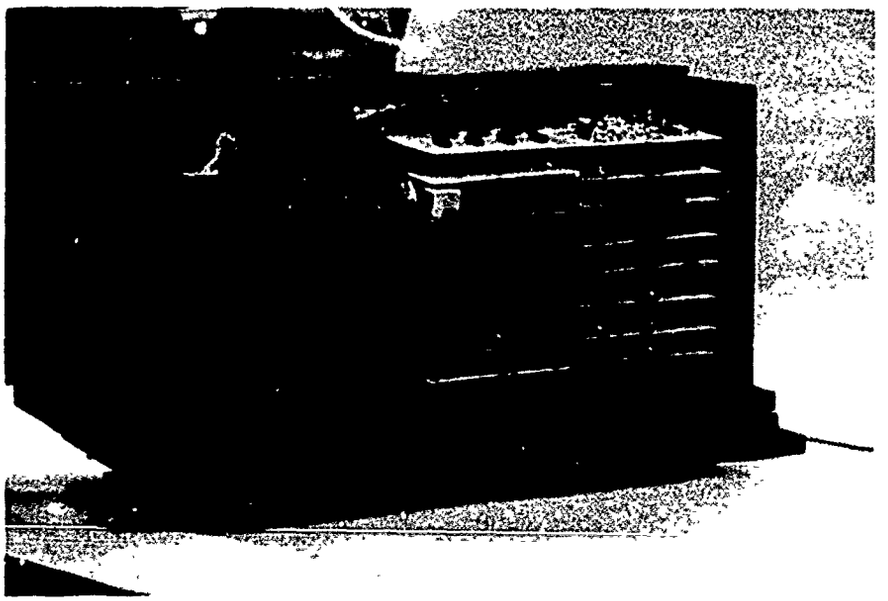

Figure II-8. Receiver, Left Side, Cover Removed

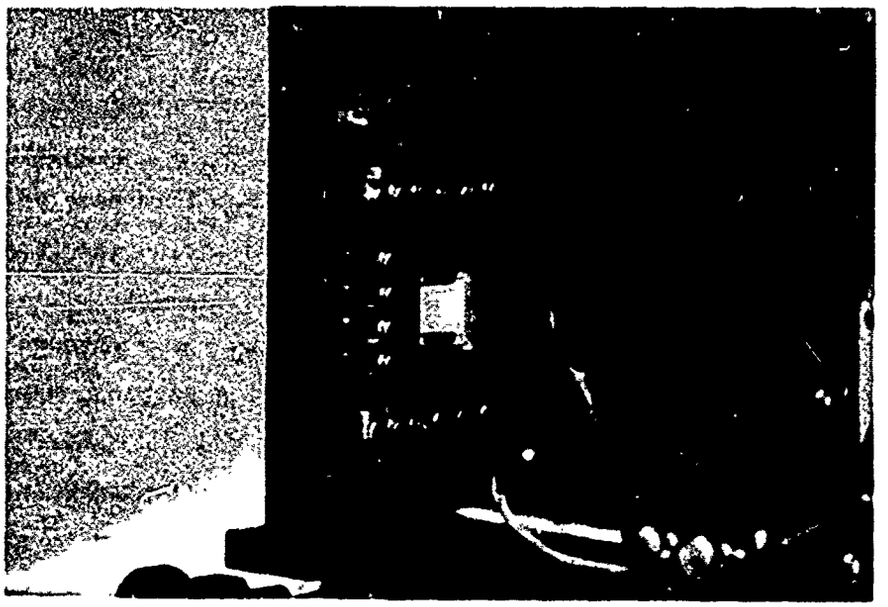

Figure II-9. Receiver, Diode Array

distance to the target and differences in target reflectivity. In addition, since the received signal is a random variable, consideration must be given to the expected fluctuation in signal about the mean value so as not to limit the signal unnecessarily and distort the apparent statistics.

Our previous analysis[16] assumes that the received fields are Gaussian distributed. This in turn leads to an exponential probability density function for the intensity which can be written as

$$P_I(\alpha) = \frac{1}{\langle I \rangle} \; e^{-\frac{\alpha}{\langle I \rangle}}$$

Now if the value of intensity for which saturation of the electronics occurs is given by b, then the fraction of samples T on the average for which the receiver will be saturated is given by

$$T = \int_0^b P_I(\alpha) d\alpha = 1 - e^{-\frac{b}{\langle I \rangle}}$$

A reasonable value for T is 0.95. This corresponds to $b/\langle I \rangle = 3$. The gain can then be set such that the mean is approximately equal to one-third of the peak allowable output. This same principle can be used to set the gain even if the distribution is not exponential.

The system gain is set by the operator through the use of switches on the control panel. Once the gain has been properly set, both the average received intensity and the target range are monitored by the computer and if a significant change is detected, the operator is alerted. It is anticipated that future versions of the software will incorporate automatic gain setting by the processor.

III. ANALYSIS

The work that follows is based on the extended Huygens-Fresnel formulation and includes the effects of the turbulent atmosphere on the laser beam as it propagates to the target and on the speckle as it propagates back to the receiver. Formulations are developed for the variance, covariance, time-delayed covariance, slope of the time-delayed covariance and the temporal power spectral density of the received intensity. These formulations include the effects of the log-amplitude covariance as well as the wave structure function and represent a significant extension of previous work.[17]

The source, target, and receiver configuration is shown in Figure III-1. The present analysis is confined to the case of a TEM_{00} laser illuminator. It is assumed that the source and target are much smaller than the path length L, that the distance between the receiver and source is much smaller than the path length, and that the outgoing and returning radiation experience independent turbulence regions. The last assumption is thought to be correct for the case of a perfectly diffuse target when the received fields are jointly Gaussian (low turbulence) or when phase perturbation is the dominant turbulence effect. It may not be a valid assumption when the log-amplitude perturbation is dominant and the validity of the last assumption under this condition remains to be investigated.

The source amplitude distribution can be written as

$$U_o(\bar{r}) = U_o \exp\left(-\frac{r^2}{2\alpha_o^2} - \frac{ikr^2}{2F}\right) \qquad \text{(III-1)}$$

where α_o and F are the characteristic beam radius and focal length respectively. The field at the target before scattering from the target then is written from the extended Huygens-Fresnel principle[18,19] as

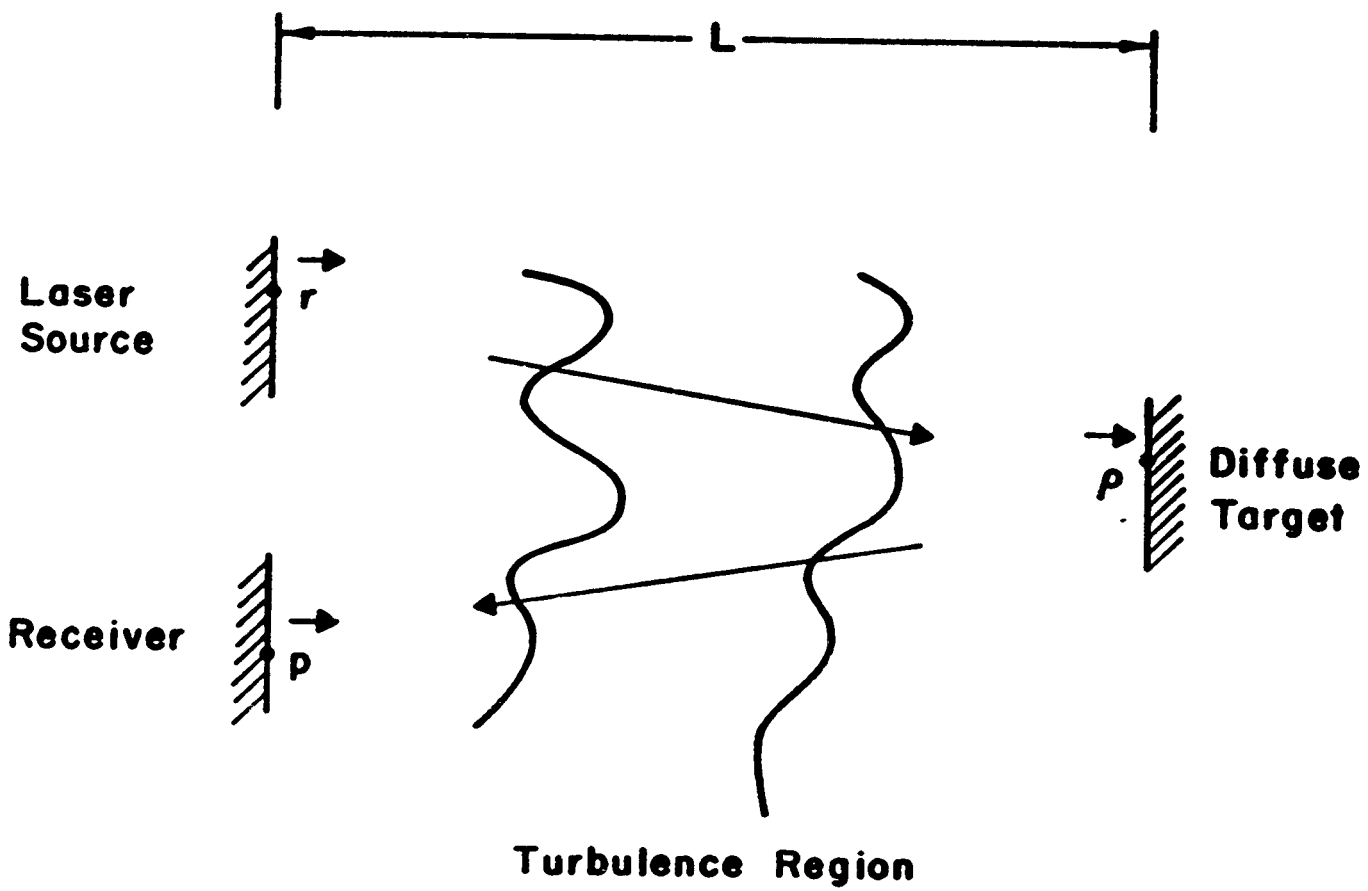

Figure III-1 Illuminator, Target, and Receiver Configuration

$$U'(\bar{\rho}) = \frac{ke^{ik\left[L + \frac{\rho^2}{2L}\right]}}{2\pi iL} \int U_o(\bar{r}) \exp\left[\frac{ik(r^2 - 2\bar{r}\cdot\bar{\rho})}{2L} + \psi_1(\bar{\rho},\bar{r})\right] d\bar{r} \tag{III-2}$$

where ψ_1 describes the effects of the random medium on the propagation of a spherical wave from the source to the target.

The field at the receiver is written by reapplying the Huygens-Fresnel principle to the field at the target and

$$U(\bar{p}) = \frac{ke^{ik\left[L + \frac{p^2}{2L}\right]}}{2\pi iL} \int U(\bar{\rho}) \exp\left[\frac{ik}{2L}(\rho^2 - 2\bar{\rho}\cdot\bar{p}) + \psi_2(\bar{p},\bar{\rho})\right] d\bar{\rho} \tag{III-3}$$

where $U(\bar{\rho})$ is the field at the target after scattering from the target. Utilizing (III-2) and (III-3), the statistics of the received intensity can be formulated.

Since all of the desired statistics can be derived from the time-delayed correlation function, it will be developed first. The time-delayed correlation function for the intensity can be expressed as

$$\begin{aligned} B_I(\bar{p}_1,\bar{p}_2,\tau) &= \langle U(\bar{p}_1,o)U^*(\bar{p}_1,o)U(\bar{p}_2,\tau)U^*(\bar{p}_2,\tau)\rangle \\ &= \left(\frac{k}{2\pi L}\right)^4 \iiiint d\bar{\rho}_1 d\bar{\rho}_2 d\bar{\rho}_3 d\bar{\rho}_4 \langle U(\bar{\rho}_1,o)U^*(\bar{\rho}_2,o) \\ &\quad U(\bar{\rho}_3,\tau)U^*(\bar{\rho}_4,\tau)\rangle \exp\left[\frac{ik}{2L}\left(\rho_1^2 - \rho_2^2 + \rho_3^2 - \rho_4^2\right.\right. \\ &\quad \left.\left. - 2\bar{p}_1\cdot(\bar{\rho}_1 - \bar{\rho}_2) - 2\bar{p}_2\cdot(\bar{\rho}_3 - \bar{\rho}_4)\right)\right] \\ &\quad H(\bar{\rho}_1, \bar{\rho}_2, \bar{\rho}_3, \bar{\rho}_4; \bar{p}_1, \bar{p}_2; \tau) \end{aligned} \tag{III-4}$$

where

$$H = \langle \exp[\psi(\bar{\rho}_1, \bar{\rho}_1, o) + \psi^*(\bar{\rho}_1, \bar{\rho}_2, o) + \psi(\bar{\rho}_2, \bar{\rho}_3, \tau) + \psi^*(\bar{\rho}_2, \bar{\rho}_4, \tau)] \rangle$$

$$= \exp\left[-\frac{1}{2}(D_{12} - D_{13} + D_{14} + D_{23} - D_{24} + D_{34}) + 2C_{\chi_{13}} + 2C_{\chi_{24}}\right] \quad \text{(III-5)}$$

and where the wave structure function and the log-amplitude covariance function are given by[19,7]

$$\frac{1}{2}D_{ij} = \frac{1}{2}\left\langle\left[\psi(\bar{\rho}_i, \bar{\rho}_i, t_i) - \psi(\bar{\rho}_j, \bar{\rho}_j, t_j)\right]^2\right\rangle$$

$$= \frac{2.91}{2} Lk^2 \int_o^1 C_n^2(t) \left| t(\bar{\rho}_j - \bar{\rho}_i) - \bar{V}(t_j - t_i) + (1 - t)(\bar{\rho}_j - \bar{\rho}_i) \right|^{5/3} dt \quad \text{(III-6)}$$

and

$$C_{\chi_{ij}} = 0.132\,\pi^2 k^2 L \int_o^1 dt\; C_n^2(t) \int_o^\infty du\, u^{-8/3} \sin^2\left[\frac{u^2 t(1-t)L}{k}\right] J_o\left[u\left| t(\bar{\rho}_j - \bar{\rho}_i) - \bar{V}(t_j - t_i) + (\bar{\rho}_j - \bar{\rho}_i)(1 - t)\right|\right] \quad \text{(III-7)}$$

and where $\bar{\rho}_2 = \bar{\rho}_1$; $\bar{\rho}_3 = \bar{\rho}_2$; $\bar{\rho}_4 = \bar{\rho}_2$; $t_1 = t_2 = o$; and $t_3 = t_4 = \tau$. The dummy variable t represents the distance from the source to the field point normalized by the total path length L. Since we are considering propagation from the transmitter to the target and also from the target to the receiver, care must be taken to distinguish between this normalized path

length variable for the two directions of propagation if the formulations are to be valid in the case of non-uniform turbulence C_n^2 and crosswind velocity $\bar{V}$ and if a wind weighting function is to be developed. Consequently, we will use t to indicate the normalized distance from the target to the receiver and t will be replaced by 1 - t when propagation is from the transmitter to the target. It should be noted that (III-6) is good to order n_2 and that (III-7) is good only to order n_1. In addition there are also some limitations to (III-5) which are discussed in Appendix A where it is derived.

After scattering from the target, the fields are jointly Gaussian.[20,21] Consequently,

$$\langle U(\bar{\rho}_1, o)\, U^*(\bar{\rho}_2, o)\, U(\bar{\rho}_3, \tau) U^*(\bar{\rho}_4, \tau)\rangle$$

$$= \langle U(\bar{\rho}_1, o) U^*(\bar{\rho}_2, o)\rangle\langle U(\bar{\rho}_3, \tau) U^*(\bar{\rho}_4, \tau)\rangle$$

$$+ \langle U(\bar{\rho}_1, o) U^*(\bar{\rho}_4, \tau)\rangle\langle U(\bar{\rho}_3, \tau) U^*(\bar{\rho}_2, o)\rangle \qquad \text{(III-8)}$$

For the case of a perfectly diffuse target, (III-8) becomes[17,22-27]

$$\langle U(\bar{\rho}_1, o) U^*(\bar{\rho}_2, o) U(\bar{\rho}_3, \tau) U^*(\bar{\rho}_4, \tau)\rangle$$

$$= \left(\frac{4\pi}{k^2}\right)^2 \langle I(\bar{\rho}_1, o)\rangle\langle I(\bar{\rho}_3, \tau)\rangle\, \delta(\bar{\rho}_1 - \bar{\rho}_2)\, \delta(\bar{\rho}_3 - \bar{\rho}_4)$$

$$+ \left(\frac{4\pi}{k^2}\right)^2 \langle U(\bar{\rho}_4, o) U^*(\bar{\rho}_4, \tau)\rangle\langle U(\bar{\rho}_2, \tau) U^*(\bar{\rho}_2, o)\rangle$$

$$\delta(\bar{\rho}_1 - \bar{\rho}_4)\, \delta(\bar{\rho}_3 - \bar{\rho}_2) \qquad \text{(III-9)}$$

Using (III-9) in (III-4) and performing the $d\bar{\rho}_1$ and $d\bar{\rho}_3$ integrations, the time delayed correlation function becomes

$$B_I(\bar{\rho}, \tau) = \frac{1}{\pi^2 L^4} \iint d\bar{\rho}_2 d\bar{\rho}_4 \langle I(\bar{\rho}_2, o)\rangle\langle I(\bar{\rho}_4, \tau)\rangle\, H_1(\bar{\rho}_2, \bar{\rho}_4, \bar{\rho}_1, \bar{\rho}_2)$$

$$+ \frac{1}{\pi^2 L^4} \iint d\bar{\rho}_2 d\bar{\rho}_4 \, \langle U(\bar{\rho}_4, o) U^*(\bar{\rho}_4, \tau) \rangle \langle U(\bar{\rho}_2, \tau) U^*(\bar{\rho}_2, o) \rangle$$

$$e^{i\frac{k}{L}\bar{p} \cdot \bar{\rho}} H_2(\bar{\rho}_2, \bar{\rho}_4, \bar{p}_1, \bar{p}_2) \qquad \text{(III-10)}$$

where

$$H_1 = H\Big|_{\bar{\rho}_1 = \bar{\rho}_2;\ \bar{\rho}_3 = \bar{\rho}_4;\ \bar{p}_2 = \bar{p}_1;\ \bar{p}_3 = \bar{p}_2;\ \bar{p}_4 = \bar{p}_2}$$

$$= e^{4C_\chi(\bar{p}, \bar{\rho}, \tau)} \qquad \text{(III-11)}$$

$$H_2 = H\Big|_{\bar{\rho}_1 = \bar{\rho}_4;\ \bar{\rho}_3 = \bar{\rho}_2;\ \bar{p}_2 = \bar{p}_1;\ \bar{p}_3 = \bar{p}_2;\ \bar{p}_4 = \bar{p}_2}$$

$$= \exp\left[-\frac{1}{2}\left[2D_\psi(o, \bar{\rho}, o) - D_\psi(\bar{p}, -\bar{\rho}, \tau) + 2D_\psi(\bar{p}, o, \tau) - D_\psi(\bar{p}, \bar{\rho}, \tau)\right] + 2C_\chi(\bar{p}, -\bar{\rho}, \tau) + 2C_\chi(\bar{p}, \bar{\rho}, \tau)\right] \qquad \text{(III-12)}$$

$$\bar{p} = \bar{p}_2 - \bar{p}_1$$

$$\bar{\rho} = \bar{\rho}_4 - \bar{\rho}_2$$

and where in (III-6) and (III-7), $\bar{p}_j - \bar{p}_i = \bar{p}$; $\bar{\rho}_j - \bar{\rho}_i = \bar{\rho}$; and $t_j - t_i = \tau$. The time delayed covariance is given by

$$C_I(\bar{p}, \tau) = B_I(\bar{p}, \tau) - \langle I(\bar{p}) \rangle^2 \qquad \text{(III-13)}$$

where from previous work[17]

$$\langle I(\bar{\rho})\rangle = \frac{1}{\pi L^2}\int d\bar{\rho}\ \langle I(\bar{\rho})\rangle \qquad \text{(III-14)}$$

Utilizing (III-13) and (III-14) in (III-10) the time delayed covariance becomes

$$C_I(\bar{\rho},\tau) = C_{I_1} + C_{I_2} = \frac{1}{\pi^2 L^4}\iint d\bar{\rho}_2 d\bar{\rho}_4 \left(e^{4C_\chi(\bar{\rho},\bar{\rho},\tau)} - 1\right)$$

$$I(\bar{\rho}_2)\rangle\langle I(\bar{\rho}_4)\rangle$$

$$+ \frac{1}{\pi^2 L^4}\iint d\bar{\rho}_2 d\bar{\rho}_4\ H_2(\bar{\rho},\bar{\rho},\tau)\ e^{i\frac{k}{L}\bar{\rho}\cdot\bar{\rho}}$$

$$\langle U(\bar{\rho}_4, o)U^*(\bar{\rho}_4,\tau)\rangle\langle U(\bar{\rho}_2,\tau)U^*(\bar{\rho}_2, o)\rangle \qquad \text{(III-15)}$$

Again utilizing the extended Huygens Fresnel principle

$$\langle U(\bar{\rho}_4, o)U^*(\bar{\rho}_4,\tau)\rangle = \left(\frac{k}{2\pi L}\right)^2 U_o^2 \iint d\bar{r}_1\, d\bar{r}_2\ \exp\left[-\left(\frac{r_1^2 + r_2^2}{2a_o^2}\right)\right.$$

$$\left. + i\,\frac{k}{2L}\left(1 - \frac{L}{F}\right)(r_1^2 - r_2^2) - i\,\frac{k}{L}\bar{\rho}_4\cdot(\bar{r}_1 - \bar{r}_2)\right]$$

$$\langle\exp\left[\psi(\bar{\rho}_4,\bar{r}_1, o) + \psi^*(\bar{\rho}_4,\bar{r}_2,\tau)\right]\rangle \qquad \text{(III-16)}$$

where

$$\langle\exp[\psi(\bar{\rho}_4,\bar{r}_1, o) + \psi^*(\bar{\rho}_4,\bar{r}_2,\tau)\rangle$$

$$= \exp\left[-\frac{1}{2}D_\psi(o,\bar{r}_2 - \bar{r}_1,\tau)\right] \qquad \text{(III-17)}$$

Now making the change of variable

$$\bar{r}_1 - \bar{r}_2 = \bar{r}$$

$$\bar{r}_1 + \bar{r}_2 = 2\bar{R}$$

in (III-16) it becomes

$$\langle U(\bar{\rho}_4, o)U^*(\bar{\rho}_4, \tau)\rangle = \left(\frac{k}{2\pi L}\right)^2 U_o^2 \iint d\bar{r}d\bar{R}\, \exp\left[-\left(\frac{r^2 + 4R^2}{4\alpha_o^2}\right)\right.$$

$$\left. + \frac{ik}{L}\left(1 - \frac{L}{F}\right)(\bar{r}\cdot\bar{R}) - i\frac{k}{L}\bar{\rho}_4\cdot\bar{r} - \frac{1}{2}D_\psi(o, -\bar{r}, \tau)\right] \quad \text{(III-18)}$$

Performing the θ_R and the R integrations,[17] (III-18) becomes

$$\langle U(\bar{\rho}_4, o)U^*(\rho_4, \tau)\rangle = \frac{1}{2\pi}\left(\frac{k}{L}\right)^2 U_o^2 \frac{\alpha_o^2}{2}\int d\bar{r}\, \exp\left[-\frac{r^2}{4\alpha_o^2}\right.$$

$$\left. - i\frac{k}{L}\bar{\rho}_4\cdot\bar{r} - \frac{1}{2}D_\psi(o, -\bar{r}, \tau) - \left[\frac{k}{L}\frac{\alpha_o}{2}\left(1 - \frac{L}{F}\right)\right]^2 r^2\right] \quad \text{(III-19)}$$

Using (III-19) in the second term of (III-15), and making the change of variable

$$\bar{\rho}_4 - \bar{\rho}_2 = \bar{\rho}$$

$$\bar{\rho}_4 + \bar{\rho}_2 = 2\bar{R}$$

it becomes

$$C_{I_2}(\bar{p}, \tau) = \left(\frac{k^2U_o^2\alpha_o^2}{4\pi^2L^4}\right)^2 \iint d\bar{r}_1 d\bar{r}_2\, \exp\left[-\left(\frac{r_1^2 + r_2^2}{4\alpha_o^2}\right)\right.$$

$$- \frac{1}{2}D_\psi(o, -\bar{r}_1, \tau) - \frac{1}{2}D_\psi(o, -r_2, -\tau)$$

$$\left. - \left[\frac{k}{L}\frac{\alpha_o}{2}\left(1 - \frac{L}{F}\right)\right]^2 (r_1^2 + r_2^2)\right]$$

$$\int d\bar{\rho}\, \exp\left[i\frac{k}{L}\bar{p}\cdot\bar{\rho} - i\frac{k}{2L}\bar{\rho}\cdot(\bar{r}_2 - \bar{r}_1)\right] H_2(\bar{\rho}, \bar{p}, \tau)$$

$$\int R dR \int d\theta_R \exp\left[-i\frac{k}{L}\bar{R}\cdot\left(\bar{r}_2+\bar{r}_1\right)\right] \qquad \text{(III-21)}$$

Now performing the θ_R and the $\bar{r}_1$ integrations,[17] (III-21) becomes

$$C_{I_2}(\bar{\rho},\tau) = \left(\frac{k}{2\pi L}\right)^2 \langle I\rangle^2 \int d\bar{r}_2 \exp\left[-\frac{r_2^2}{2\alpha_o^2} - D_\psi(o,-\bar{r}_2,\tau)\right.$$

$$\left. - 2r_2^2\left[\frac{k}{L}\,\frac{\alpha_o}{2}\left(1-\frac{L}{F}\right)\right]^2\right]\int d\bar{\rho}\, e^{i\frac{k}{L}\bar{\rho}\cdot(\bar{r}_2+\bar{\rho})} H_2(\bar{\rho},\bar{\rho},\tau) \qquad \text{(III-22)}$$

The first term in (III-15) will now be evaluated. The average intensity can be obtained by letting $\tau = o$ in (III-19) and then performing the θ_r integration. It becomes

$$\langle I(\rho_4)\rangle = \left(\frac{k}{L}\right)^2 \frac{U_o^2\alpha_o^2}{2}\int r dr\, J_o\left(\frac{k}{L}\rho_4 r\right)\exp\left[-\frac{r^2}{4\alpha_o^2}\right.$$

$$\left. - \frac{1}{2}D_\psi(o,-\bar{r},o) - \left[\frac{k}{L}\frac{\alpha_o}{2}\left(1-\frac{L}{F}\right)\right]^2 r^2\right] \qquad \text{(III-23)}$$

Using (III-23) in the first term of (III-15), and making the change of variable

$$\bar{\rho}_2 - \bar{\rho}_4 = \bar{\rho}$$

$$\bar{\rho}_4 + \bar{\rho}_2 = 2\bar{R}$$

it becomes

$$C_{I_1} = \frac{k^4 \alpha_o{}^4 U_o{}^4}{4\pi^2 L^8} \iint d\bar{\rho} d\bar{R} \left(e^{4C_\chi(\bar{\rho}, \bar{\rho}, \tau)} - 1 \right)$$

$$J_o\left(\frac{k}{L}\left|\frac{\bar{\rho}}{2} + \bar{R}\right| r_1\right) J_o\left(\frac{k}{L}\left|\bar{R} - \frac{\bar{\rho}}{2}\right| r_2\right) \iint r_1 r_2 dr_1 dr_2$$

$$\exp\left[- \frac{\left(r_1{}^2 + r_2{}^2\right)}{4\alpha_o{}^2} - \frac{1}{2} D_\psi(o, -\bar{r}_1, o) \right.$$

$$\left. - \frac{1}{2} D_\psi(o, -\bar{r}_2, o) - \left(\frac{k}{L} \frac{\alpha_o}{2} \left(1 - \frac{L}{F}\right)\right)^2 \left(r_1{}^2 + r_2{}^2\right) \right] \qquad \text{(III-24)}$$

Now performing the θ_R, R, and r integrations,[17] (III-24) becomes

$$C_{I_1}(\bar{\rho}, \tau) = \frac{\langle I \rangle^2}{2\pi} \left(\frac{k}{L}\right)^2 \iint r_2 dr_2 \, d\bar{\rho} \, J_o\left(\frac{k}{L} r_2 \rho\right) \left(e^{4C_\chi(\bar{\rho}, \bar{\rho}, \tau)} - 1 \right)$$

$$\exp\left[- \frac{r_2{}^2}{2\alpha_o{}^2} - D_\psi(o, \bar{r}_2, o) - 2\left(\frac{k}{L} \frac{\alpha_o}{2} \left(1 - \frac{L}{F}\right)\right)^2 r_2{}^2 \right] \qquad \text{(III-25)}$$

This completes the derivation of the time delayed covariance function. It is represented by the sum of equations (III-22) and (III-25).

There are four statistical quantities that are of interest and can be derived from the time delayed covariance function: the variance; covariance; power spectral density; and

the slope of the time delayed covariance function at zero time delay. The last quantity is of special interest since it is proportional to the path averaged crosswind. The other statistical quantities are needed for overall system design.

The variance can be obtained from the time delayed covariance by setting $\bar{\rho} = o$ and $\tau = o$. Under these conditions, the θ_ρ integration can be performed and the variance is given by

$$\sigma_I^2 = \langle I \rangle^2 \left(\frac{k}{L}\right)^2 \iint r_2 dr_2 \rho d\rho \exp\left[-D_\psi(o, \bar{r}_2, o) - r_2^2\left[\frac{1}{2\alpha_o^2} + 2\left(\frac{k}{L}\frac{\alpha_o}{2}\left(1 - \frac{L}{F}\right)\right)^2\right]\right]\left[2e^{4C_\chi(\rho)} - 1\right] J_o\left(\frac{k}{L}\rho r_2\right) \tag{III-26}$$

The covariance can be obtained from the time delayed covariance by setting $\tau = o$. This allows the θ_{r_2} integration to be performed in the second term and

$$C_I(\bar{\rho}) = C_{I_1}(\bar{\rho}, o) + C_{I_2}(\bar{\rho}, o)$$

where

$$C_{I_2}(\bar{\rho}, o) = \frac{\langle I \rangle^2}{2\pi}\left(\frac{k}{L}\right)^2 \iint r_2 dr_2 \exp\left[-\frac{r_2^2}{2\alpha_o^2} - D_\psi(o, -\bar{r}_2, o) - 2r_2^2\left[\frac{k}{L}\frac{\alpha_o}{2}\left(1 - \frac{L}{F}\right)\right]^2\right] \int d\bar{\rho}\, e^{i\frac{k}{L}\bar{p}\cdot\bar{\rho}} J_o\left(\frac{k}{L}\rho r_2\right) H_2(\bar{\rho}, \bar{p}, o) \tag{III-27}$$

and $C_{I_1}(\bar{p}, o)$ is given by (III-25) with $\tau = o$.

The temporal power spectral density is the Fourier transform of the time delayed covariance function evaluated at $\bar{p} = o$. Since no additional integrals can be evaluated it will not be written in detail, but it can easily be obtained from

$$S_{II}(w) = \int_{-\infty}^{\infty} e^{-jw\tau} \left[C_{I_1}(o, \tau) + C_{I_2}(o, \tau)\right] d\tau \qquad \text{(III-28)}$$

and equations (III-22) and (III-25).

The slope of the time delayed covariance function is given by

$$M_I(\bar{p}) = \frac{\partial}{\partial \tau} C_I(\bar{p}, \tau)\Big|_{\tau = o}$$

$$= \frac{\partial}{\partial \tau} C_{I_1}(\bar{p}, \tau)\Big|_{\tau = o} + \frac{\partial}{\partial \tau} C_{I_2}(\bar{p}, \tau)\Big|_{\tau = o} \qquad \text{(III-29)}$$

where the two derivatives with respect to τ can be obtained from (III-22) and (III-25). Using (III-25),

$$\frac{\partial}{\partial \tau} C_{I_1}(\bar{p}, \tau)\Big|_{\tau = o} = \frac{\langle I \rangle^2}{2\pi} \left(\frac{k}{L}\right)^2 4 \iint r_2 dr_2 d\bar{\rho}\, J_o\left(\frac{k}{L} r_2 \rho\right) e^{4C_\chi(\bar{p}, \bar{\rho}, o)}$$

$$e^{-D_\psi(o, \bar{r}_2, o)} f(r_2) \frac{\partial}{\partial \tau} C_\chi(\bar{p}, \bar{\rho}, \tau)\Big|_{\tau = o}$$

(III-30)

where

$$\frac{\partial}{\partial \tau} C_\chi(\bar{p}, \bar{\rho}, \tau)\Big|_{\tau = o} = \int_o^1 dt\ C_n^2\ \bar{V} \cdot \bar{C}_{\chi_\tau}(\bar{p}, \bar{\rho}) \qquad \text{(III-31)}$$

$$\bar{C}_{\chi_\tau}(\bar{p}, \bar{\rho}) = 0.132\ \pi^2\ k^2\ L\ \frac{(\bar{p}t + (1 - t)\bar{\rho})}{|\bar{p}t + (1 - t)\bar{\rho}|} \int_0^\infty du\ u^{-5/3}$$

$$\sin^2\left(\frac{u^2 t\ (1 - t)L}{2k}\right)\ J_1(u|\bar{p}t + (1 - t)\bar{\rho}|) \qquad \text{(III-32)}$$

and

$$f(r_2) = \exp\left[-\frac{r_2^2}{2a_o^2} - 2\left(\frac{k}{L}\frac{a_o}{2}\left(1 - \frac{L}{F}\right)\right)^2 r_2^2\right]$$

From (III-22), the second term in (III-29) becomes

$$\frac{\partial}{\partial \tau} C_{I_2}(\bar{p}, \tau)\Big|_{\tau = o} = \frac{\langle I \rangle^2}{(2\pi)^2}\left(\frac{k}{L}\right)^2 \int d\bar{r}_2\ f(r_2) \int d\bar{\rho}\, e^{i\frac{k}{L}\bar{\rho} \cdot (\bar{p} + \bar{r}_2)}$$

$$\frac{\partial}{\partial \tau}\left[e^{-D_\psi(o, -\bar{r}_2, \tau)} H_2(\bar{p}, \bar{\rho}, \tau)\right]\Big|_{\tau = o}$$

$$= \frac{\langle I \rangle^2}{(2\pi)^2}\left(\frac{k}{L}\right)^2 \int d\bar{r}_2\ f(r_2) \int d\bar{\rho}\, e^{i\frac{k}{L}\bar{\rho} \cdot (\bar{p} + r_2)}$$

$$e^{-D_\psi(o, r_2, o)} H_2(\bar{p}, \bar{\rho}, o) \int_o^1 dt\ C_n^2\ \bar{V}$$

$$\cdot\Big[-\bar{D}_{\psi\tau}\ (o, -\bar{r}_2) + \frac{1}{2}\,\bar{D}_{\psi\tau}\ (\bar{\rho}, -\bar{\rho}) - \bar{D}_{\psi\tau}\ (\bar{\rho}, o)$$

$$+\frac{1}{2}\,\bar{D}_{\psi\tau}\ (\bar{\rho}, \bar{\rho}) + 2\,\bar{C}_{\chi_\tau}(\bar{\rho}, -\bar{\rho}) + 2C_{\chi_\tau}\ (\bar{\rho}, \bar{\rho})\Big] \qquad \text{(III-33)}$$

where use has been made of

$$\frac{\partial}{\partial\tau}\,D_{\psi}\ (\bar{\rho}, \bar{\rho}, \tau)\Big|_{\tau = o} = \int_o^1 dt\ C_n^{\,2}\ \bar{V}\cdot\bar{D}_{\psi\tau}(\bar{\rho}, \bar{\rho}) \qquad \text{(III-34)}$$

and

$$\bar{D}_{\psi\tau}(\bar{\rho}, \bar{\rho}) = -9.70\ Lk^2\ \frac{(\bar{\rho}t + (1-t)\bar{\rho})}{|\bar{\rho}t + (1-t)\bar{\rho}|}^{1/3} \qquad \text{(III-35)}$$

The θr_2 integration can now be performed on all but one term and the slope becomes

$$M_I(\bar{\rho}) = \frac{\langle I\rangle^2}{2\pi}\left(\frac{k}{L}\right)^2\int_o^1 dt\ C_n^{\,2}\ \bar{V}\cdot\bar{W} \qquad \text{(III-36)}$$

where the vector wind weighting function $\bar{W}$ is given by

$$\bar{W} = \iint r_2 dr_2\ d\bar{\rho}\ f(r_2)\ J_o\left(\frac{k}{L}\bar{\rho}r_2\right)e^{-D_\psi(o,\ \bar{r}_2,\ o)}$$

$$\Big[4e^{4C_\chi(\bar{\rho},\ \bar{\rho},\ o)}\bar{C}_{\chi\tau}(\bar{\rho}, \bar{\rho}) + H_2(\bar{\rho}, \bar{\rho}, o)e^{i\frac{k}{L}\bar{\rho}\cdot\bar{\rho}}\left(\frac{1}{2}\,\bar{D}_{\psi\tau}(\bar{\rho}, -\bar{\rho})\right.$$

$$\left.-\bar{D}_{\psi\tau}(\bar{\rho}, o) + \frac{1}{2}\,\bar{D}_{\psi\tau}(\bar{\rho}, \bar{\rho}) + 2C_{\chi_t}(\bar{\rho}, -\bar{\rho}) + 2C_{\chi_\tau}(\bar{\rho}, \bar{\rho})\right)\Big]$$

$$- \frac{1}{2\pi} \iint d\bar{r}_2 \, f(r_2) d\bar{\rho} \, e^{i\frac{k}{L} \bar{\rho} \cdot (\bar{p} + \bar{r}_2) - D_\psi(o, \bar{r}_2, o)}$$

$$H_2(\bar{p}, \bar{\rho}, o) \, \bar{D}_{\psi_\tau}(o, -\bar{r}_2) \qquad \text{(III-37)}$$

The results of this section are summarized in Table III-1 which lists the pertinent equation numbers for such statistical quantity that has been developed.

Table III-1. Equation Summary

Statistic	Pertinent Equations
Time Delayed Covariance	15, 22, 25, 6, 7, 12
Variance	26, 6, 7
Covariance	27, 25, 6, 7, 12
Power Spectral Density	28, 22, 25, 6, 7, 12
Slope	36, 37, 6, 7, 12, 32, 35

Numerical evaluation of these equations is considered in Section IV.

A physical interpretation of the variance and covariance reveals the mechanisms involved in speckle propagation through turbulence in a particularly illuminating manner.

The variance, (III-26), heuristically may be expressed as

$$\sigma_{I_n}^2 = 2 e^{4\gamma\sigma_\chi^2} - 1 \qquad \text{(III-38)}$$

which in cases where $4\gamma\sigma_\chi^2 \ll 1$ can be written

$$\sigma_{I_n}^2 \approx 1 + 8\gamma\sigma_\chi^2 \qquad \text{(III-39)}$$

In these expressions, σ_χ^2 is the log amplitude variance for a point source propagating over the target-receiver path, and

γ (≤ 1) is the "source smoothing factor" associated with the nonzero spot size (S) on the target. Mathematically, γ relates to the integration over (ρ) in (III-26), with the spot size ($S = \frac{L}{k\alpha_0}$ or $\frac{L}{k\rho_0}$) coupled through r. For a small transmitter (or defocused spot), or strong turbulence, the target spot will be $S \gtrsim \sqrt{L/k}$ and γ will be less than unity. In the limit of strong turbulence, $\gamma \approx 0$ while for weak turbulence, $\sigma_\chi^2 = 0$; either extreme results in a unity variance.

A quantitative estimate of γ may be obtained as follows. From published results[28] for the variance with an extended incoherent source, we know that in weak scattering

$$\gamma \sim \left(\frac{S}{\sqrt{L/k}}\right)^{-7/3} \qquad \text{(III-40)}$$

The smoothing in the strong scattering case is conjectured to be

$$\gamma \sim \left(\frac{S}{\rho_o}\right)^{-2} \qquad \text{(III-41)}$$

This source or target-spot smoothing is analogous to finite-receiver smoothing.

The expressions corresponding to (III-38) and (III-39) for an incoherent source are

$$\sigma_{I_n}^2 = e^{4\gamma\sigma_\chi^2} - 1 \qquad \text{(III-42)}$$

$$\sigma_{I_n}^2 \approx 4\gamma\sigma_\chi^2 \qquad \text{(III-43)}$$

It may be seen that the unity baseline and half the remaining term in (III-39) arise from the source coherence or speckle phenomenon, whether controlled by the target (weak turbulence) or atmosphere (strong turbulence). Alternatively, we may observe that the unity term arises strictly from phase randomization,

with associated exponential irradiance statistics, while the remaining term represents the effects of nonzero amplitude perturbations, with associated log normal statistics.

To further illustrate these considerations, let us consider the large, focused transmitter condition ($\alpha_o >> \sqrt{L/k}$). We first consider the weak turbulence condition ($\rho_o > \alpha_o > \sqrt{L/k}$, in which the transmitter is able to operate in an essentially diffraction-limited manner. The target-spot is small, i.e. such that the receiver is in the far-field of the spot, and the situation is much like that of a point source ($\sigma_\chi^2 << 1, \gamma = 1$). There is however one major difference from the point-source case: we assume a good statistical (ensemble) average of the field, which as a practical matter means that the target is moved slowly so that the (large) speckles sweep past the receiver. (If the transmitter, target, and receiver were rigidly fixed, the receiver would see part of one speckle, and the turbulence fluctuations would be that of a point source, with purely log normal statistics and a variance of $e^{4\sigma_\chi^2} - 1 \approx 4\sigma_\chi^2$). The resultant variance is essentially unity, with small turbulence-caused fluctuations superimposed on the basic speckles that would be present in the absence of the atmosphere. The irradiance statistics will be nearly exponential.

We now let the turbulence strength grow until "saturation" or multiple scattering sets in. The peak value of σ_χ^2 is known[29] to be approximately 0.6, occurring when ρ_o is on the order of $\sqrt{L/k}$. The target spot will no longer be diffraction limited ($\alpha_o > \rho_o \approx \sqrt{L/k}$), and hence γ will be less than unity. The exact value of the peak variance can only be determined from a full numerical evaluation of (III-26), including the detailed effects of saturation on $C_\chi(\bar{\rho})$; the statistics will be a composite of log normal and exponential distributions. As the turbulence strength grows

further, σ_χ^2 decreases ("super-saturation") to the limit ≈ 0.17; also the target-spot grows indefinitely, so that γ decreases to zero in the limit. The variance therefore decreases back to unity, with exponential statistics.

We now consider the covariance case, again for a focused transmitter. For the coherent term given by (III-27) if C_χ is neglected and either α_o or ρ_o is much smaller than the other and also smaller than $\sqrt{L/k}$, the corresponding limitation on r in the integrand couples through the Bessel term and exponential to imply a similar limitation on p. This gives a closed-form covariance result which is that obtained with the assumption of joint gaussian field statistics[16,17] and

$$C_{I_n}(\bar{p}) = e^{-p^2/2\alpha_o^2 - 4(p/\rho_o)^{5/3}} \qquad \text{(III-44)}$$

Hence the covariance arising from the coherent term is generally exponential[16] with a scale equal to the smaller of α_o or ρ_o (target and atmospheric speckles respectively). In the event that α_o and ρ_o are comparable, the complete expression must be used and the field statistics are marginally (but not joint) gaussian.[16,17] In the event that C_χ is non-negligible, the covariance scale relating to the coherent term is largely unaffected.

We now consider the incoherent term (III-25). If the target spot is small compared to $\sqrt{L/k}$, i.e. α_o and $\rho_o \gg \sqrt{L/k}$, the large range of r in the integrand will couple through J_o to hold ρ small in C_χ. Hence the covariance scale will be determined by $C_\chi(p,0)$ and will be $\sqrt{L/k}$ as expected for a small target spot. However, for a large target spot (S), the ρ range in the integrand will be large and the p-scale in C_I will be "smeared" to the order of S. This effect is consistent with the incoherent-source results of

Ref. 8, and can be argued from simple geometry: for two receivers separated by a small distance relative to the source size, the source-turbulence configuration over the paths to each respective receiver will be highly correlated. The statistics associated with the incoherent term are log normal, although the log amplitude is not jointly normal except for weak fluctuations.

IV. NUMERICAL EVALUATION

The theoretical formulations for the statistics of the received intensity must be reduced to numbers as required for system evaluation and design. Standard numerical integration techniques proved too time consuming due to the three-fold integrations required, and Monte-Carlo techniques would not work due to the form of the integrand and the interdependency of integration limits. However, a major analytical breakthrough has been achieved which greatly simplifies the formulations while retaining a complete description of the mechanisms involved. We are now able to reduce the formulations to numbers for comparison with the cw experimental results and for design purposes.

The variance and covariance have the following form for the case of uniform turbulence

$$\sigma_I^2 = \langle I \rangle^2 \left(\frac{k}{L}\right)^2 \int_0^\infty \int_0^\infty r\,dr\,\rho\,d\rho \left[2e^{4C_\chi(\rho)} - 1\right] J_o\left(\frac{k}{L}\,\rho r\right) f_2(r) \qquad \text{(IV-1)}$$

$$C_I(\bar{\rho}) = C_{I_1}(\bar{\rho}) + C_{I_2}(\bar{\rho}) \qquad \text{(IV-2)}$$

where

$$C_{I_1}(\bar{\rho}) = \langle I \rangle^2 \frac{1}{2\pi} \left(\frac{k}{L}\right)^2 \iiint d\theta\,dr\,d\rho\; r\rho \left(e^{4C_\chi(\bar{\rho},\,\bar{\rho})} - 1\right) J_o\left(\frac{k}{L}\,r\rho\right) f_2(r) \qquad \text{(IV-3)}$$

$$C_{I_2}(\bar{\rho}) = \langle I \rangle^2 \frac{1}{2\pi} \left(\frac{k}{L}\right)^2 e^{-2\left(\frac{\rho}{\rho_o}\right)^{5/3}} \iiint d\theta$$

$$\mathrm{d}r\mathrm{d}\rho\; r\rho\; f_1(\bar{\rho},\bar{p})\; J_o\left(\frac{k}{L} r\rho\right)\; f_2(r) \tag{IV-4}$$

$$f_1(\bar{\rho},\bar{p}) = \exp\left[i\frac{k}{L}\bar{\rho}\cdot\bar{p} - 2\left(\frac{\rho}{\rho_o}\right)^{5/3} + \frac{8}{3}\frac{1}{\rho_o{}^{5/3}}\right.$$

$$\left[\int_0^1 \mathrm{d}t\,|\bar{p}t + (1-t)\bar{\rho}|^{5/3} + \int_0^1 \mathrm{d}t\,|\bar{p}t - (1-t)\bar{\rho}|^{5/3}\right]$$

$$\left. + 2\,C_\chi(\bar{\rho},\bar{p}) + 2\,C_\chi(\bar{\rho},-\bar{p})\right] \tag{IV-5}$$

$$f_2(r) = \exp\left[-r^2\left(\frac{1}{2\alpha_o{}^2} - 2\left(\frac{k}{L}\frac{\alpha_o}{2}\left(1-\frac{L}{F}\right)\right)^2\right) - 2\left(\frac{r}{\rho_o}\right)^{5/3}\right] \tag{IV-6}$$

Each of the integrands contains the term $rJ_o\left(\frac{k}{L} r\rho\right)\; f_2(r)$. Our approach is to expand $f_2(r)$ in a Fourier-Bessel series and then make use of

$$\int_o^\infty rJ_o(\alpha r)J_o(\beta r)\mathrm{d}r = \frac{2\delta(\alpha-\beta)}{\alpha+\beta} \tag{IV-7}$$

to simplify the integration. The series is given by

$$f_2(r) = \sum_m b_m\, J_o\left(\frac{P_m}{A} r\right) \tag{IV-8}$$

where

$$b_m = \frac{2}{A^2 J_1^2(P_m)} \int_o^A xf(x)\, J_o\left(\frac{P_m}{A} X\right)\, \mathrm{d}x \tag{IV-9}$$

and

$$J_o(P_m) = 0$$

This expansion can be done because $f_2(r)$ becomes negligible for some value of r that is easily calculated and does not depend on the other integration variables. In addition, the shape of $f_2(r)$ allows it to be represented by only a few terms in the series. Our experience indicates that for problems of interest to this program, around six terms in the series yields accurate results.

Using (IV-7) - (IV-9), the variance and covariance become

$$\sigma_I^2 = \langle I \rangle^2 \sum_m b_m \left[2e^{4C_\chi\left(\frac{L}{k}\frac{P_m}{A}\right)} - 1 \right] \qquad \text{(IV-10)}$$

$$C_I = \frac{\langle I^2 \rangle}{2\pi} \sum_m b_m \int d\theta \left[e^{4C_\chi\left(\frac{L}{k}\frac{P_m}{A},\, p,\, \theta\right)} - 1 - 2\left(\frac{P}{\rho_o}\right)^{5/3} + e^{f_1\left(\frac{L}{k}\frac{P_m}{A},\, p,\, \theta\right)} \right] \qquad \text{(IV-11)}$$

where θ is the angle between $\bar{P}$ and $\bar{\rho}$. The net effect of the above work is in the case of the variance to reduce a twofold integration to a set of well defined onefold integrations; and in the case of the covariance to reduce a rather involved threefold integration with interacting limits to a well defined onefold integration plus a set of well defined onefold integrations.

Equations (IV-10) and (IV-11) which contain the log-amplitude covariance function given to order n_1 by[7]

$$C_\chi(\bar{\rho}, \bar{p}) = 0.132\,\pi^2 k^2 C_n^2 \int_0^1 dt \int_0 du^{-8/3} \sin^2\left(\frac{u^2 t(1-t)L}{2k}\right)$$

$$J_0\left(u|\bar{p}t + \bar{\rho}(1-t)|\right) \qquad \text{(IV-12)}$$

Evaluation of (IV-12) is now the limiting factor in generating numbers from the variance and covariance formulations. For the variance, $\bar{p} = 0$ and (IV-12) can be represented by a six term series. This has allowed us to develop an efficient program that readily computes the variance. This program was used to generate the analytic, unsaturated variance curves shown in Section V which discusses the cw experimental results.

For the covariance, $\bar{p}$ is not zero and (IV-12) is not easily reduced to a simple form. The technique used by Fried[30] for the case $\bar{p} = 0$ unfortunately does not work when $\bar{p} \neq 0$ and for the parameter values of interest. Several other expansion techniques have been attempted, but so far we have not been able to reduce (IV-12) to a more tenable form. We are still working to resolve this problem. Meanwhile, a twofold Gaussian quadrature numerical integration is being used to evaluate (IV-12). It is relatively time consuming because for problems of practical interest, many cycles of the SIN squared term must be included in the range of integration. However, we have been able to generate some numerical values for the unsaturated covariance as shown in Section V.

Equation (IV-12) holds only for non-saturated turbulence conditions. For saturated turbulence there is presently no two source log-amplitude covariance formulation available for use in (IV-11) and one must be developed. However, Clifford and Yura[31] have developed a single source ($\bar{p} = 0$) formulation.

For strongly saturated turbulence it is given by

$$C_\chi(\bar{\rho}) = 0.42\,\alpha^{5/3}\int_0^1 du \int_0^\infty dq\, e^{-q}\, J_0\left\{\left(\frac{3.347}{\alpha}\right) q^{-3/5}\,\frac{\rho}{\rho_0}\right\} \qquad \text{(IV-13)}$$

where the parameter α is determined from a knowledge of the saturated value of the normalized variance of the intensity for a spherical wave. Using unity as the saturated limit, we have

$$C_\chi(0) = .17329 = 0.42\,\alpha^{5/3}\int_0^1 du \int_0^\infty dq e^{-q}$$

and the value for α is ≈ 0.588. Equation (IV-13) then becomes

$$C_\chi(\bar{\rho}) = .17329 \int_0^\infty dq e^{-q} \int_0^1 du\, J_0\left(5.693\, uq^{\,3/5}\,\frac{\rho}{\rho_0}\right) \qquad \text{(IV-14)}$$

Equation (IV-14) has been evaluated using standard numerical integration techniques and used in conjunction with (IV-10) to evaluate the variance under saturated conditions. The results are shown in Section V.

Equations (IV-10) and (IV-11) should be valid for all turbulence conditions. However, this is only true if the right form for the log-amplitude covariance function and the wave structure function are used. There is currently no simple formulation available for these quantities valid in the transition region.

V. CW EXPERIMENT

The experimental observation and measurement of statistical properties of the intensity after reflection from a diffuse or quasi-diffuse target and propagation through atmospheric turbulence are presented in this section. The purpose of the experiments, definition of the parameters and measurements of interest and the experimental design will be discussed. In addition, the results of experiments performed to date, including the relationship to recent analytical and numerical work will be presented.

The observation of scattering from a coherently illuminated diffuse target, is simply illustrated in Figure III-1 showing the source (laser), target and the receiver coplanar with the source. The source and receiver are separated by a distance that is large compared to the scales of interest in the received intensity such as a_0 (transmitter radius), $\sqrt{L/k}$, and ρ_0, and very small compared to the source-receiver and target separation. The experiments described below involve the measurement of statistical quantities discussed analytically in previous Sections and other reports.[16] These include the probability distribution function of the irradiance, the normalized variance, and the spatial covariance function. In situ atmospheric parameters including temperature, pressure, wind velocity and C_n^2 were also monitored during the data collection.

The experimental system is schematically illustrated in Figure V-1. The laser is an argon ion laser operating at 0.488 μm and yielding approximately 700 milliwatts of power. The transmitted beam is amplitude modulated at 100 kHz using a photo elastic modulator and a calcite polarizer. Scotchlite paper is used as the target material because of its high gain in comparison with a true Lambertian reflector. Laboratory

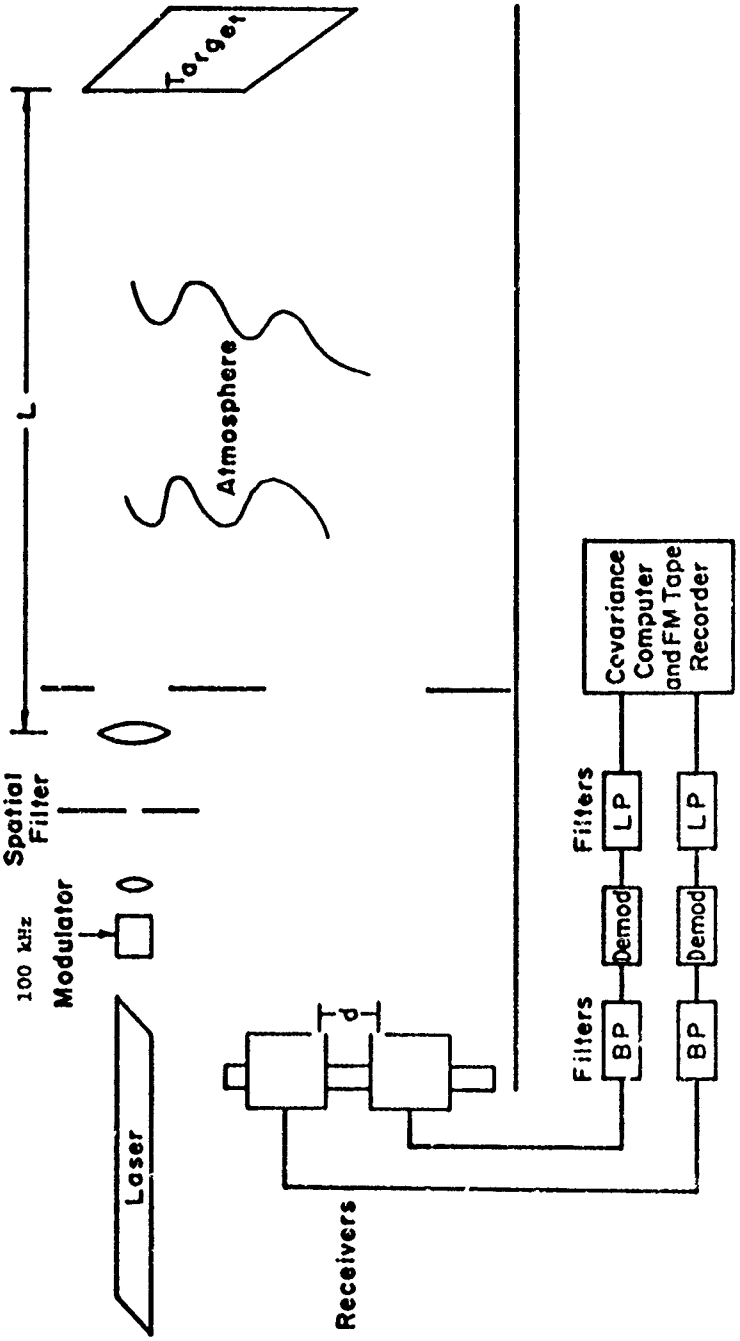

Figure V-1 Experimental Design

experiments were conducted verifying the 'diffuse' nature of the reflection from a scotchlite target. This requires that the spot size on the target be large compared to the bead size of the target material and was always true in the atmospheric experiments conducted. The receivers consist of two S-20 photomultiplier tubes followed by 10 kHz bandpass filters, synchronous demodulators, and Bessel low pass filters with switchable bandwidths between 800 Hz and 2.8 kHz. All of the statistical data reduction was done on a digital computer.

Initial experiments using a HeNe laser at 0.6328 microns over a short path indicated excellent agreement between the experimental results and the theory under low turbulence conditions. As predicted by the theory, a normalized variance equal to unity was observed. Initial experiments with the argon ion laser however produced normalized variance values of the order of 0.3. This was significantly lower than expected. However, the covariance results were substantially in agreement with the theory. The low normalized variance was related to the bandwidth of the argon ion laser which is of the order of 10 gigahertz. This translates to a coherence length of approximately 3 cm. Because the illuminated spot size at the target is of the order of centimeters, the very short coherence length of the laser will cause a decrease in the ability of light from different points on the target to interfere with a resultant decrease in the observed normalized variance. Consequently, the laser was modified to include a temperature stabilized etalon which limits the bandwidth to that of a single mode. The results for the normalized variance later in this section indicate that this modification does solve the coherence problem observed in the initial experiments.

A further recent modification to the experimental system consisted of the addition of a telescope to the front of the

receivers. The actual size of the receivers is 2 mm and the minimum separation is 4.5 mm. Under high turbulence conditions, ρ_o could become small enough that the covariance function measurements would be smoothed and increased because of the size of the detectors, and the variance measurements would be decreased by aperture smoothing over several speckles. Two telescopes were constructed which could be set onto the receiver to reduce the effective receiver size and decrease the effective minimum receiver separation. The effects of the telescopes are summarized in Table V-1.

	Magnification	Receiver Size (mm)	Minimum Separation (mm)	Relative Received Power
no telescope	1	2.0	4.5	1.0
with telescope	1.7	1.18	2.65	0.35
with telescope	3.1	0.38	1.45	0.10

Table V-1 Effect of Receiver Telescopes

The use of the telescopes of course decreased the average power received and thus a compromise was required between the observation of desired conditions and the limitations of the receiver to maintain suitable signal to noise ratios.

Each experiment consisted of a series of recordings of the irradiance at two points in the receiver plane separated by a variable distance. From these recordings, probability distribution functions (PDF) were computed from a single channel, and covariance curves were constructed by measuring the correlation coefficient between the two signals for different separations.

Figures V-2 and V-3 show typical PDF calculations from the speckle measurements for a focused transmitter and

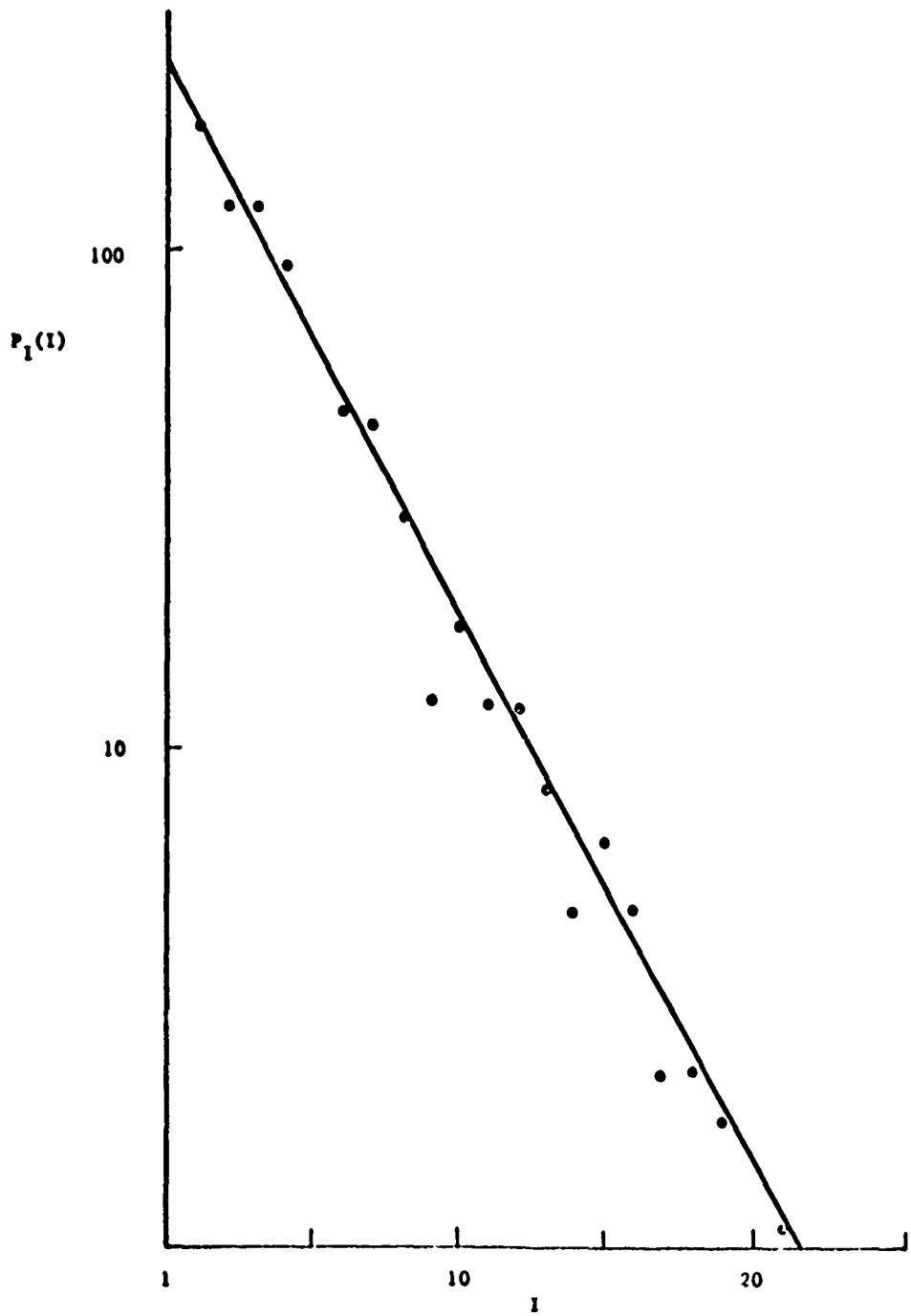

Figure V-2 Measured Probability Distribution of Irradiance, Weak Turbulence (L = 500 m, $\sigma_{I_N}^2$ = 1.02).

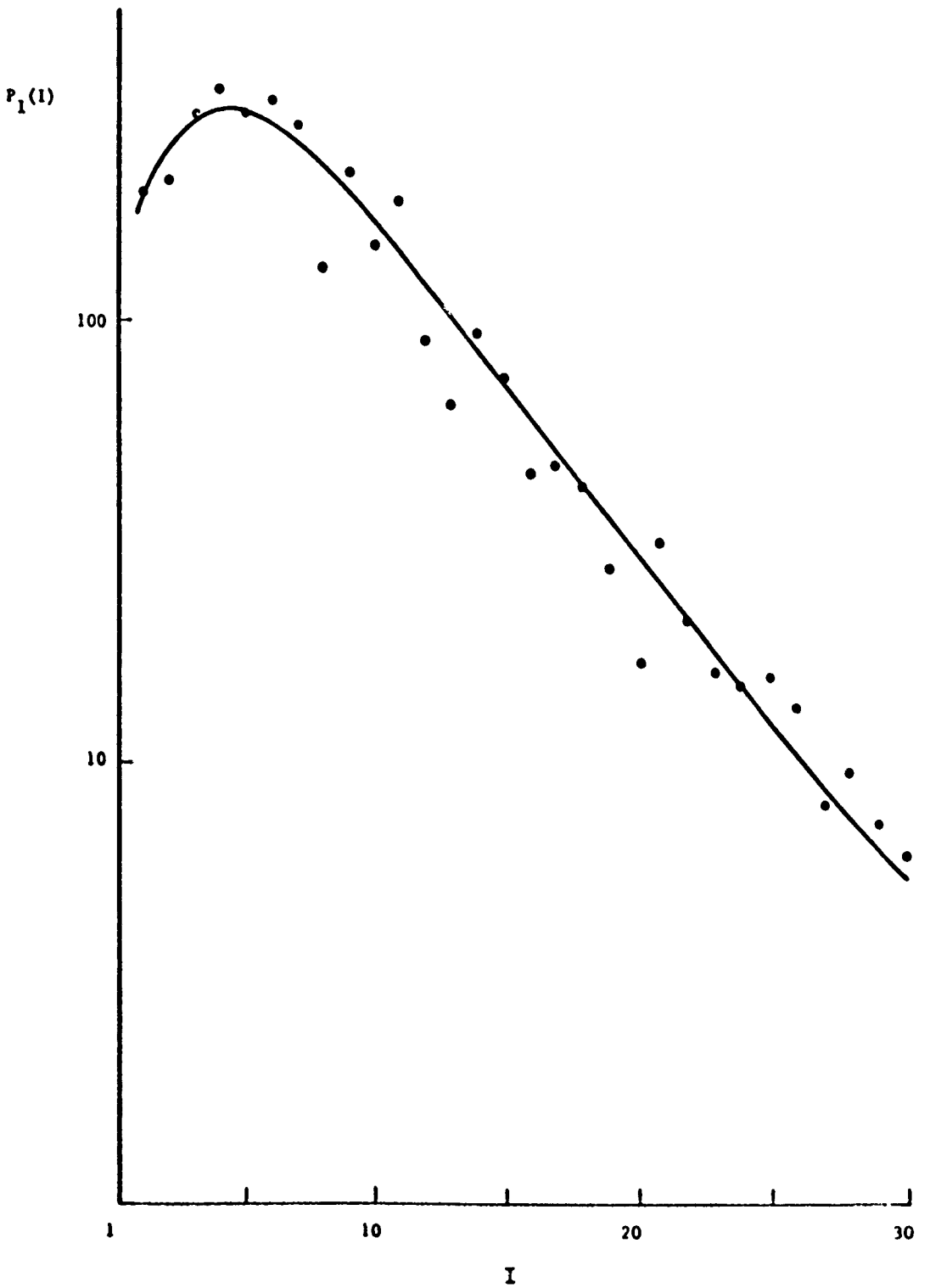

Figure V-3 Measured Probability Distribution of Irradiance, Strong Turbulence (L = 500 m, $\sigma_{I_N}^2 = 1.2$).

path length (L) = 500 m. The first of these figures is a low turbulence condition ρ_o ($\approx$ 10 cm) > α_o (1.3 cm) > $\sqrt{L/k}$ (0.62 cm) and thus target speckles would be expected to predominate. The expected PDF under these conditions is an exponential distribution.[16] A corresponding exponential distribution is plotted in the figure and the figure is well within the scatter of the experimental points. The calculated normalized variance is 1.02 as compared to the value of unity predicted by the theory. Figure V-3 shows the results for a higher turbulence case where the log-amplitude perturbation is important. The PDF in this case shows a marked deviation from exponential at low and high values of received intensity. This was expected since the total perturbation in this case is the result of the combination of two processes one of which is log-normally distributed. The measured normalized variance in this case is 1.2.

Measurements of the normalized variance $\sigma_{I_N}^2$ over a wide range of turbulence levels are shown in V-4. At very low turbulence levels ($C_n^2 \leq 10^{-15}$ $m^{-2/3}$) and high turbulence levels ($C_n^2 \geq 2 \times 10^{-13}$ $m^{-2/3}$), $\sigma_{I_N}^2$ is generally near unity as predicted by both the simple theory and the phase dominance theory. The intermediate region shows an increase in $\sigma_{I_N}^2$ above unity as predicted by the complete theory. Also shown in this figure are the results of numerical evaluations of $\sigma_{I_N}^2$ including terms containing $C_\chi(p)$ (log-amplitude covariance function). The left-hand curve was calculated using a form of $C_\chi(p)$ valid under low turbulence (unsaturated) conditions. The right-hand curve was similarly derived using a high turbulence model for $C_\chi(p)$. While not showing particularly good quantitative agreement at intermediate turbulence levels, the theoretical formulation coupled with the experimental results have provided us a good understanding of the physical mechanisms involved in this problem.

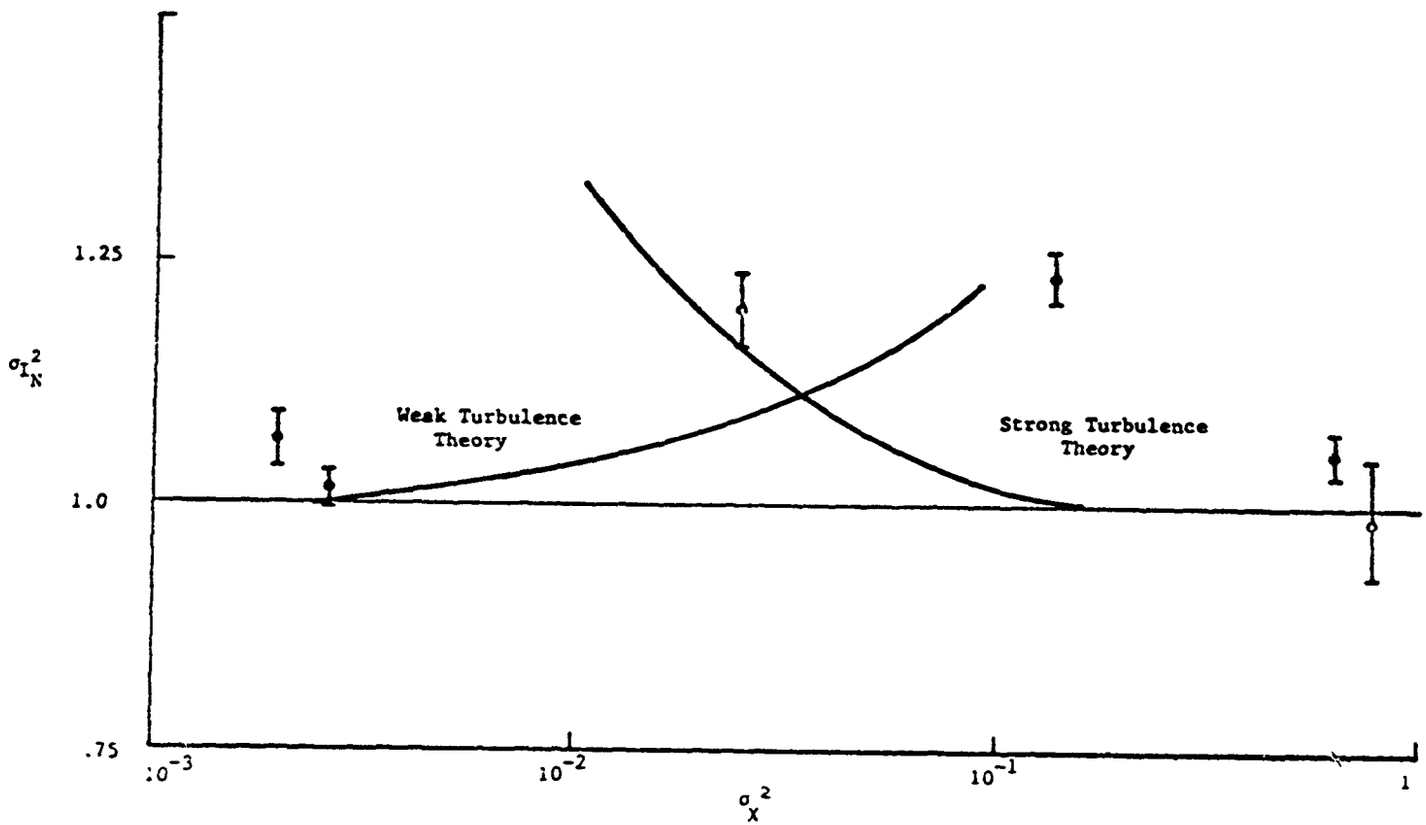

Figure V-4 Normalized Variance for a Focused Transmitter vs. Log Amplitude Variance for Point Source. (Etalon Inserted) L = 500 m.

Results of typical measurements of the covariance functions are shown in Figures V-5 through V-10 for a range of turbulence conditions and for two values of pathlength. Low turbulence conditions, such as seen in Figures V-5 through V-8 show broad covariance curves described well by the Joint Gaussian theory. As the turbulence level increases and ρ_0 approaches α_0, the covariance curves narrow as seen in Figures V-9 and V-10 and differ considerably from that predicted by the joint Gaussian theory. However, as shown in Figure V-10, there is excellent agreement between these measurements and the complete theory.

To date, excellent progress has been made in verifying our theoretical formulations with cw experimental measurements. The next step in this effort is to verify the time delayed statistics from which the crosswind is derived.

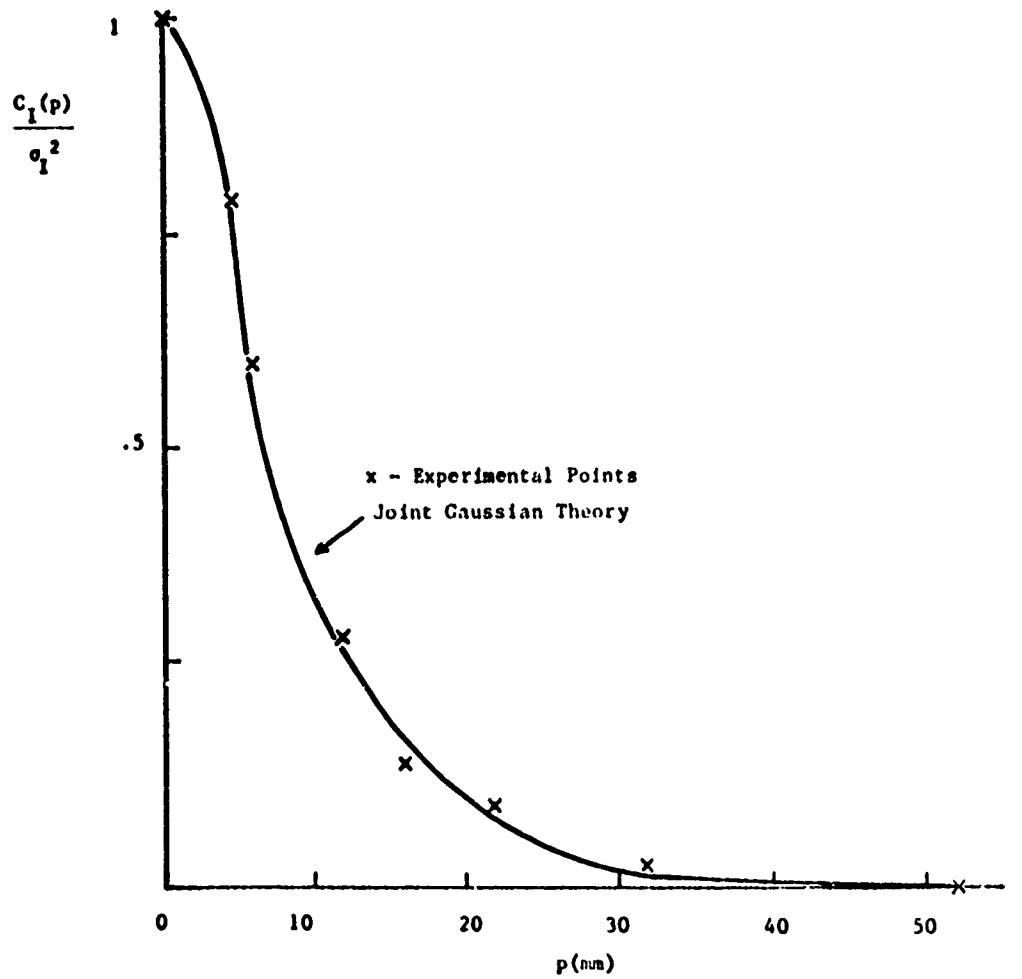

Figure V-5 Covariance for Focused Transmitter, Weak Turbulence. (L = 500 m, ρ_o = 11.5 cm, $\sqrt{L/k}$ = 6.2 mm, α_o = 1.35 cm)

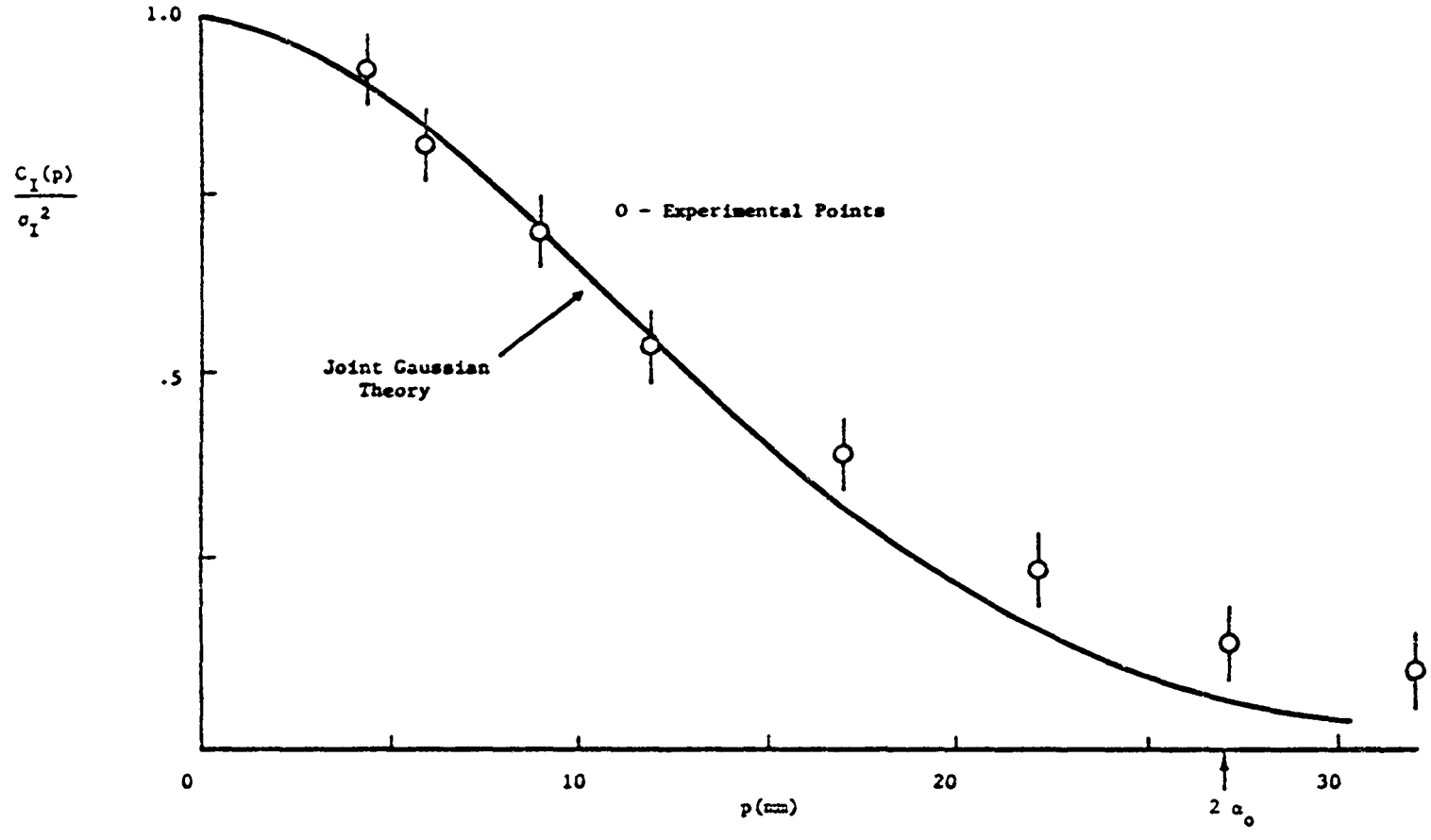

Figure V-6 Covariance for Focused Transmitter, Weak turbulence. (L = 910 m, ρ_o = 7.1 cm, $\sqrt{L/k}$ = 8.4 mm, α_o = 1.35 cm.)

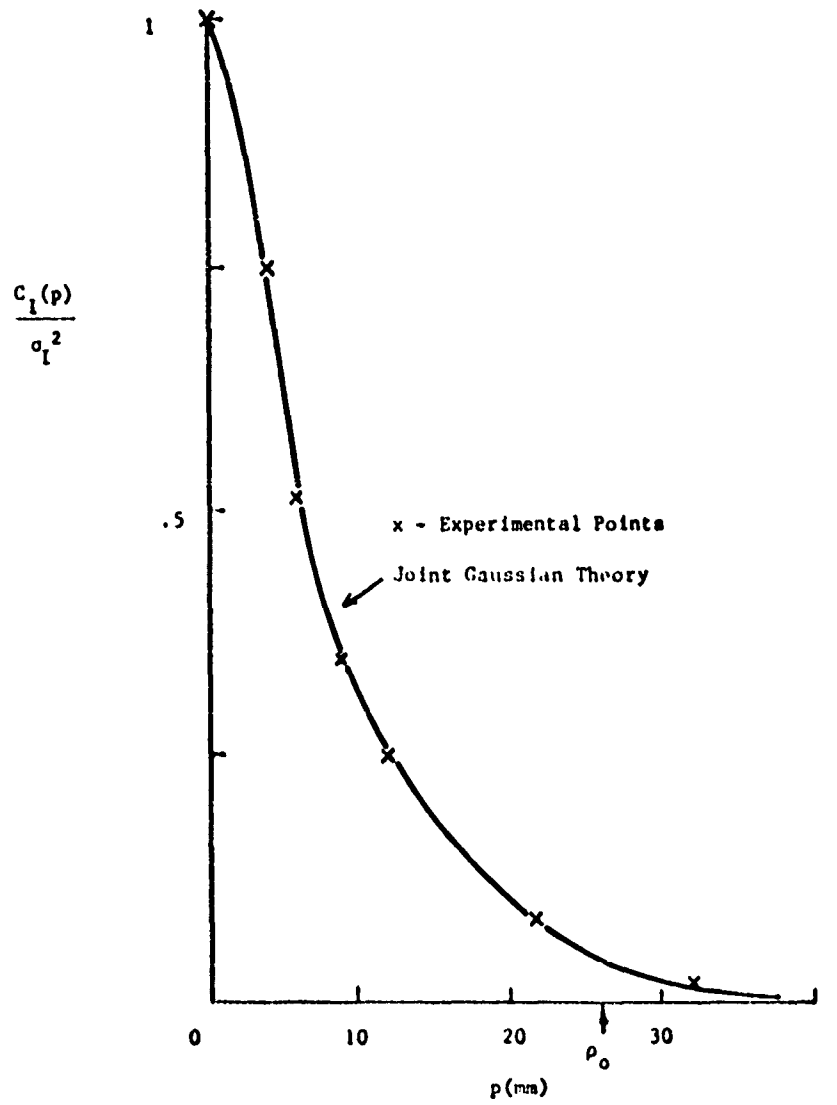

Figure V-7 Covariance for a Focused Transmitter, Moderate Turbulence. (L = 500 m, ρ_o = 2.6 cm, $\sqrt{L/k}$ = 6.2 mm, α_o = 1.35 cm.)

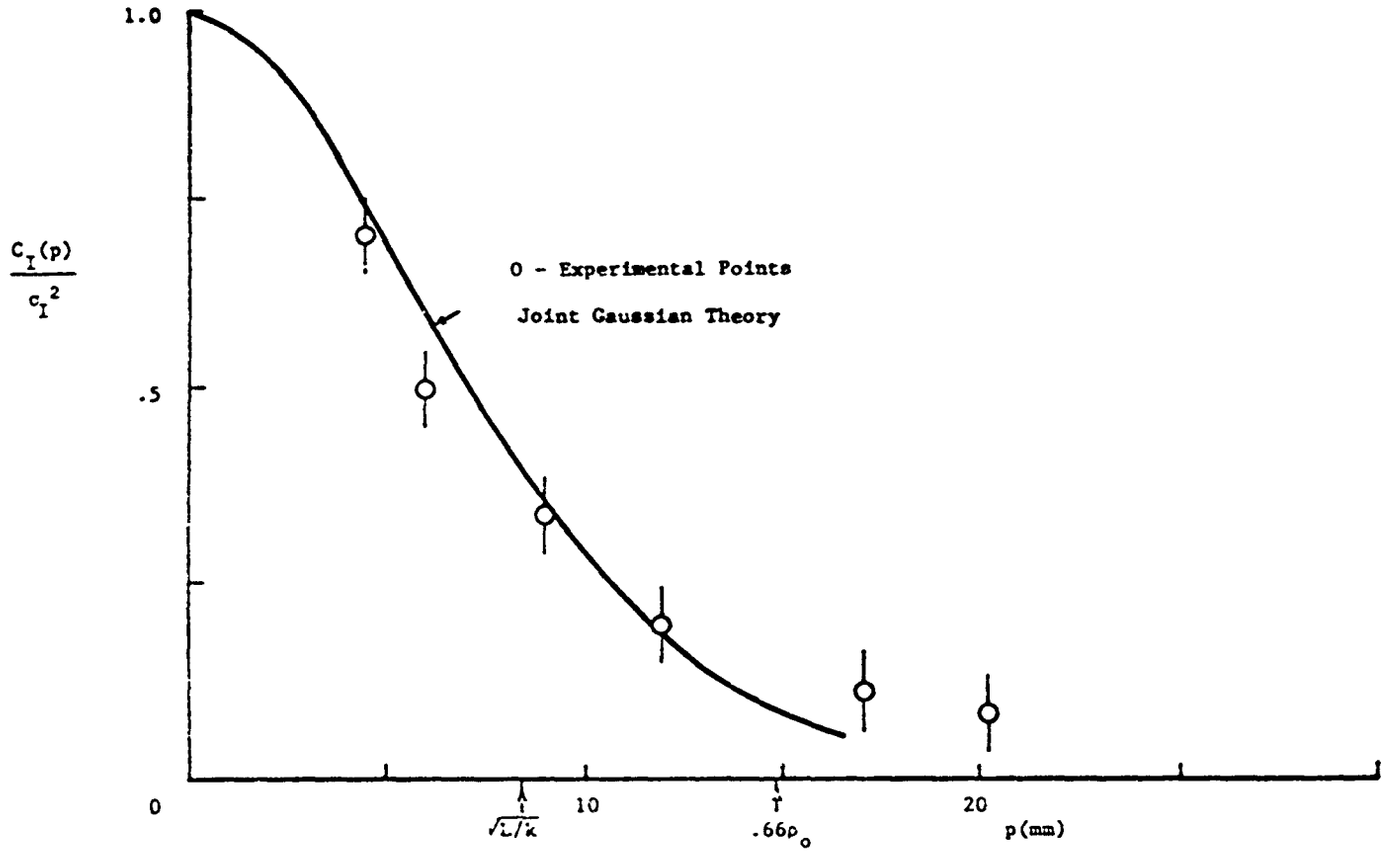

Figure V-8 Covariance for Focused Transmitter, Moderate Turbulence. (L = 910 m, ρ_o = 2.3 cm, $\sqrt{L/k}$ = 8.4 mm, α_o = 1.35 cm.)

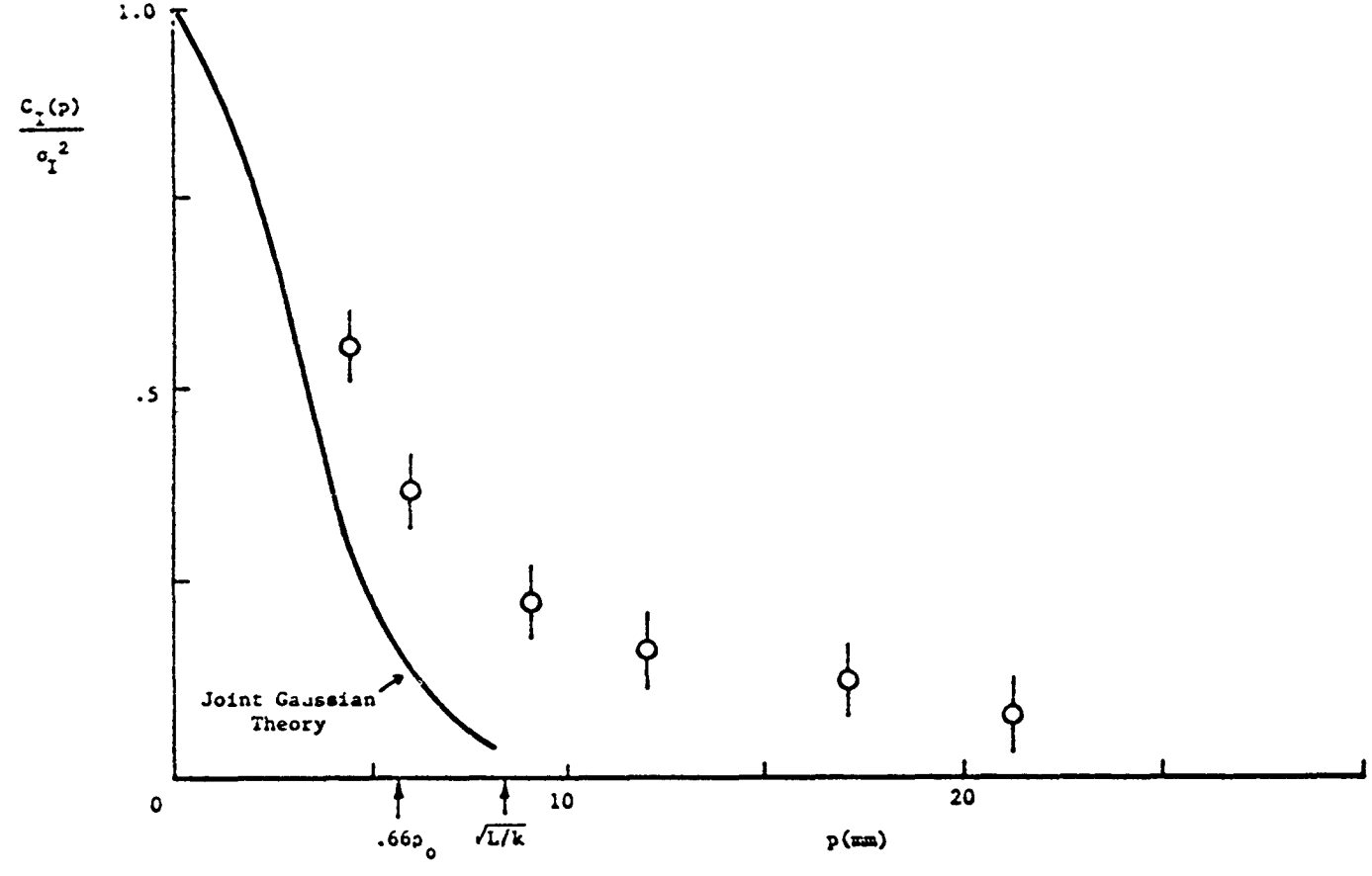

Figure V-9 Covariance for Focused Transmitter, Strong Turbulence. (L = 910 m, ρ_o = 9.6 mm, $\sqrt{L/k}$ = 8.4 mm, α_o = 1.35 cm.)

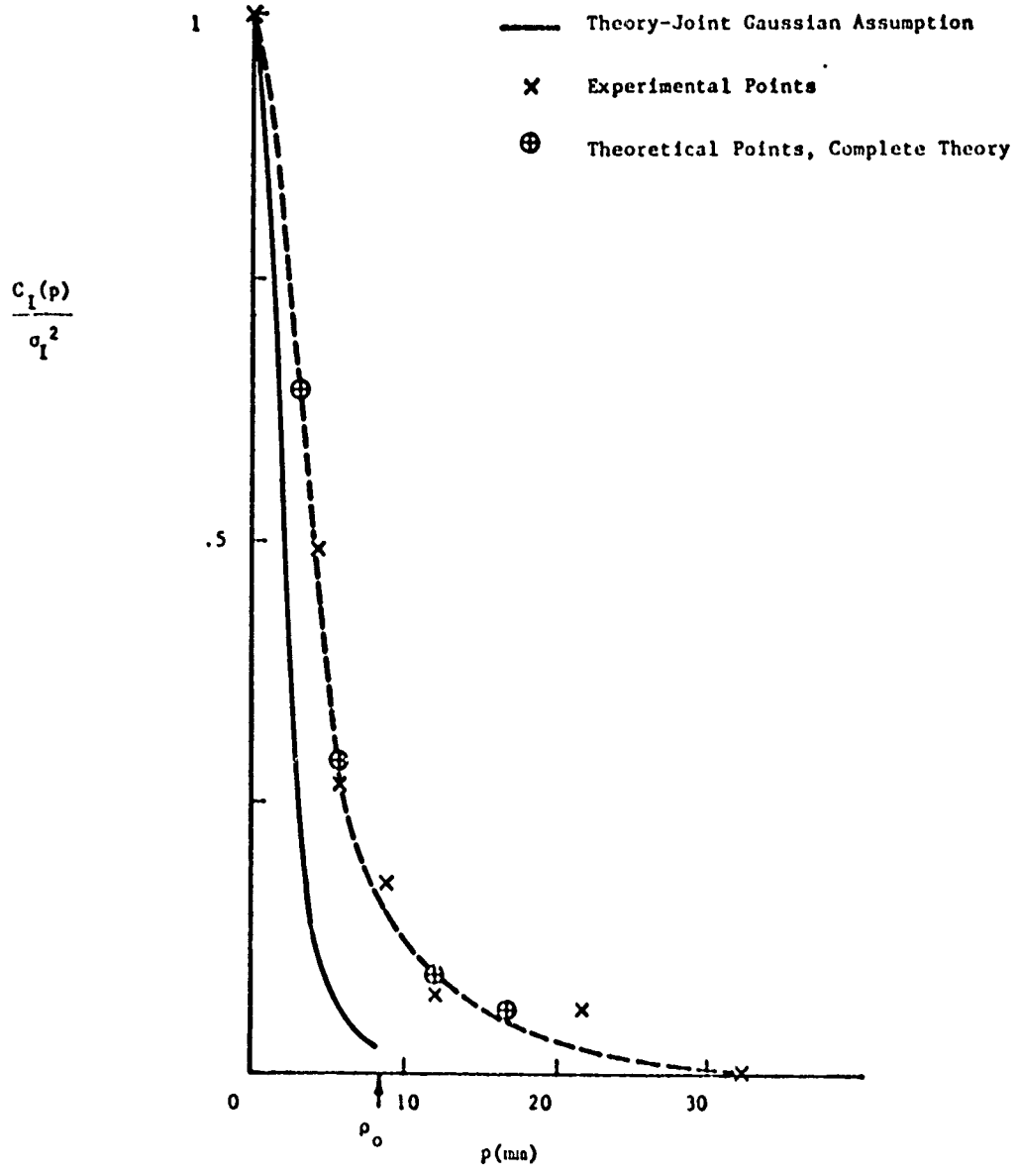

Figure V-10 Covariance for Focused Transmitter, Strong Turbulence. (L = 500 m, ρ_o = 8.4 mm, $\sqrt{L/k}$ = 6.2 mm, α_o = 1.35 cm.)

REFERENCES

1. Walters, D. L., August 1975, "Crosswind Weighting Functions for Direct-Fire Projectiles," U.S. Army Electronics Command, Research and Development Report ECOM-5570, Atmospheric Sciences Laboratory, White Sands Missile Range, New Mexico 88002.

2. Lawrence, R. S., G. R. Ochs, and S. F. Clifford, 1972, "The Use of Scintillations to Measure Average Wind Across a Light Beam," Appl. Opt., 11, 239.

3. Ochs, G. R., and G. F. Miller, 1972, "Pattern Velocity Computers - Two Types Developed for Wind Velocity Measurements by Optical Means," Rev. of Sci. Instrum., 43, 879.

4. Pries, T. H., and E. T. Young, 1974, "Evaluation of a Laser Crosswind System," United States Army Electronics Command Research and Development Technical Report, ECOM-5546.

5. Ochs, G. R., S. F. Clifford, and T. I. Wang, 1973, "A Feasibility Study of an Optical Crosswind Monitor," NOAA Technical Memorandum WPL-10.

6. Clifford, S. F., G. R. Ochs and Ting-i Wang, September 1974, "Theoretical Analysis and Experimental Evaluation of a Prototype Passive Sensor to Measure Crosswinds," NOAA Technical Report ERL 312-WPL 35.

7. Wang, Ting-i, S. F. Clifford and G. R. Ochs, 1974, "Wind and Refractive - Turbulence Sensing Using Crossed Laser Beams," Appl. Opt., 13, 2602.

8. Clifford, S. F., G. R. Ochs and Ting-i Wang, 1975, "Optical Wind Sensing by Observing the Scintillations of a Random Scene," Appl. Opt., 14, 2844.

9. Ochs, G. R., S. F. Clifford, and Ting-i Wang, 1976, "Laser Wind Sensing: the Effects of Saturation of Scintillation," Appl. Opt., 15, 403.

10. Smith, J., 1973, "Folded Path Weighting Function for a High Frequency Spherical Wave," J. Opt. Soc. Am., 63, 1095.

11. Smith, J., T. H. Pries, K. J. Skipka, and M. A. Hamiter, 1972, "High Frequency Plane-Wave Filter Function for a Folded Path," J. Opt. Soc. Am., 62, 1183.

12. Goldberg, I. I., November 1968, "Considerations of Automatic Tracker Application in Combat Vehicles," Department of the Army, Frankford Arsenal Memorandum Report M68-37-1, Philadelphia, Pa. 19137.

13. Kerr, J. R., 1967, "Microwave-Bandwidth Optical Systems," Proc. IEEE, 55, 1686.

14. Holmes, J. F. and J. R. Kerr, July 1974, "Experimental Pulsed Laser, Remote Crosswind Measurement System -- Feasibility Study and Design," U.S. Army Electronics Command, Research and Development Technical Report ECOM 74-0094-1, Atmospheric Sciences Laboratory, U.S. Army Electronics Command, White Sands Missile Range, New Mexico 88002.

15. Holmes, J. F., J. R. Kerr, et al., January 1975, "Experimental Pulsed Laser, Remote Crosswind Measurement System -- Feasibility Study and Design (Part II)," U.S. Army Electronics Command, Research and Development Technical Report ECOM75-1, Atmospheric Sciences Laboratory, U.S. Army Electronics Command, White Sands Missile Range, New Mexico 88002.

16. Holmes, J. F., J. R. Kerr, et al., September 1975, "Experimental Pulsed Laser, Remote Crosswind Measurement System -- Feasibility Study and Design (Part III)," U.S. Army Electronics Command, Research and Development Technical Report ECOM75-1, Atmospheric Sciences Laboratory, U.S. Army Electronics Command, White Sands Missile Range, New Mexico 88002.

17. Lee, M. H., J. Fred Holmes, and J. R. Kerr, 1976, "Statistics of Speckle Propagation Through the Turbulent Atmosphere," J. Opt. Soc. Am., 66, 1164.

18. Lutomirski, R. F., and H. T. Yura, "Propagation of a Finite Optical Beam in an Inhomogeneous Medium," Applied Optics, 10, 1652 (1971).

19. Yura, H. T., "Mutual Coherence Function of a Finite Cross Section Optical Beam Propagating in a Turbulent Medium," Applied Optics, 11, 1399 (1972).

20. Teich, M. C., "Homodyne Detection of Infrared Radiation from a Moving Diffuse Target," Proc. IEEE, 57, 786 (1969).

21. George, N., and A. Jain, "Space and Wavelength Dependence of Speckle Intensity," Appl. Phys., 4, 201 (1974).

22. Goodman, J. W., "Some Effects of Target-Induced Scintillation on Optical Radar Performance," Proc. IEEE, 53, 1688 (1965).

23. Lowenthal, S., and H. Arsenault, "Image Formation for Coherent Diffuse Objects: Statistical Properties," J. Opt. Soc. Am., 60, 1478 (1970).

24. Deitz, P. H., "Image Information by Means of Speckle-Pattern Processing," J. Opt. Soc. Am., 65, 279 (1975).

25. Estes, L. E., and R. Boucher, "Temporal and Spatial-Intensity-Interferometer Imaging Through a Random Medium," J. Opt. Soc. Am., 65, 760 (1975).

26. Lahart, M. J., and A. S. Marathay, "Image Speckle Patterns of Weak Diffusers," J. Opt. Soc. Am., 65, 769 (1975).

27. Beran, M. J., and G. B. Parrent, Theory of Partial Coherence, Prentice-Hall, New Jersey, 1964.

28. R. F. Lutomirski, et al, Degradation of Laser Systems by Atmospheric Turbulence, RAND Report R-1171-ARPA/RC, June 1973.

29. R. S. Lawrence and J. W. Strobehn, "A Survey of Clear-Air Propagation Effects Relevant to Optical Communications," Proc. IEEE, 58, 1523 (1970).

30. Fried, D. L., "Propagation of a Spherical Wave in a Turbulent Medium," J. Opt. Soc. Am., 57, 175 (1967).

31. Clifford, S. F., and H. T. Yura, "Equivalence of Two Theories of Strong Optical Scintillation," J. Opt. Soc. Am., 64, 1641 (1974).

32. R. L. Fante, "On The Imaging of Incoherent Objects in a Turbulent Medium," Air Force Cambridge Research Laboratories, Technical Report AFCRL-TR-75-0546, Hanscom AFB, Massachusetts 01731. 14 October 1975.

33. J. B. Thomas, An Introduction to Applied Probability and Random Processes, (John Wiley & Sons, New York, 1971).

34. H. Cramer, Mathematical Methods of Statistics, (Princeton University Press, Princeton, New Jersey, 1966).

35. J. M. Wozencraft and I. M. Jacobs, Principles of Communication Engineering, (John Wiley & Sons, New York, 1965).

36. V. I. Tatarski, Wave Propagation in a Turbulent Medium, (McGraw-Hill, New York, 1961).

37. R. E. Hufnagel and H. R. Stanley, "Modulation Transfer Function Associated with Image Transmission Through Turbulent Media," J. Opt. Soc. Am., 54, 52 (1964).

38. R. F. Lutomirski and H. T. Yura, "Wave Structure Function and Mutual Coherence Function of an Optical Wave in a Turbulent Atmosphere," J. Opt. Soc. Am., 61, 482 (1971).

39. D. L. Fried, "Atmospheric Modulation Noise in an Optical Heterodyne Receiver," IEEE Trans. on Quantum Electronics, QE-3, 213, June 1967.

40. R. L. Fante, "Electromagnetic Beam Propagation in Turbulent Media," Proc. IEEE, 63, 1669 (1975).

41. M. E. Gracheva and A. S. Gurvich, "On strong fluctuations of the intensity of light when propagating in the lower layer of the atmosphere," Izv. Vyssh. Ucheb. Zaved. Radiofiz., vol. 8, pp. 717-724, 1965.

42. M. E. Gracheva, "Research into the statistical properties of the strong fluctuations of light when propagated in the lower layer of the atmosphere." Izv. Vyssh. Ucheb. Zaved. Radiofiz., vol. 10, pp. 775-787, 1967.

43. A. S. Gurvich, M. A. Kallistratova, and N. S. Time, "Fluctuations of the parameters of a laser light wave propagating in the atmosphere," Radiofizika, vol. 11, pp. 1360-1370, 1968.

44. M. E. Gracheva, A. S. Gurvich, and M. A. Kallistratova, "Measurements of the variance of 'strong' intensity fluctuations of laser radiation in the atmosphere," Izv. Vyssh. Ucheb. Zaved. Radiofiz., vol. 13, pp. 55-60, 1970.

45. G. E. Meyers, M. P. Keister, Jr., and D. L. Fried, "Saturation of scintillation," J. Opt. Soc. Amer., 59, 4, pp. 491-492 (1969).

46. G. R. Ochs and R. S. Lawrence, "Saturation of laser-beam scintillation under conditions of strong atmospheric turbulence," J. Opt. Soc. Amer., 59, pp. 226-227 (1969).

47. W. B. Johnson, "Turbulence-induced 'supersaturation' of laser scintillation observed over a 3.5-kilometer horizontal range," Trans. Amer. Geophys. Union, 50, 4, p. 158 (1969) (abstract only).

48. G. M. B. Bouricius and S. F. Clifford, "Experimental study of atmospherically-induced phase fluctuations in an optical signal," J. Opt. Soc. Amer., (1970).

49. A. S. Gurvich and M. A. Kallistratova, "Experimental investigations of fluctuations of arrival angle of light under the conditions of strong fluctuations of intensity," Radiofizika, 11, pp. 66-71 (1968).

50. R. L. Fante, "Some Results on the Effect of Turbulence on Phase-Compensated Systems," JOSA, 66, 730 (1976).

APPENDIX A. GENERALIZED POINT SOURCE MUTUAL COHERENCE FUNCTION

The extended Huygens-Fresnel[18-19] approach is frequently utilized for determining the moments of an electromagnetic field after propagation through a turbulent medium. Crucial to the use of this method is the availability of an appropriate point source mutual coherence function. It is the purpose of this Appendix to develop a generalized n^{th} order mutual coherence function that can be used in the extended Huygens-Fresnel integral to generate moments of any order.

The generalized n^{th} order spherical wave mutual coherence function is defined as[19]

$$H(\bar{\rho}_1, \bar{\rho}_2, \ldots \bar{\rho}_{2n}; \bar{p}_1, \bar{p}_2 \ldots \bar{p}_{2n}) = \langle \exp[\psi(\bar{\rho}_1, \bar{p}_1) + \psi^*(\bar{\rho}_2, \bar{p}_2) + \ldots \psi(\bar{\rho}_{2n-1}, \bar{p}_{2n-1}) + \psi^*(\bar{\rho}_{2n}, \bar{p}_{2n})] \rangle \quad (1)$$

where $\psi = \chi + i\phi$, $\bar{\rho}_i$ corresponds to a source point in the transmitter plane and $\bar{p}_i$ corresponds to an observation point in the receiver plane. In the work that follows, ψ will be treated as a complex, jointly normal random variable. With ψ normally distributed, then $\langle \chi \rangle = -\sigma_\chi^2$ and $\langle \chi\phi \rangle = 0$.[32] It should be noted that this is not an additional assumption, but the result of assuming ψ to be jointly normal. The implication of this assumption on ψ is discussed in the summary paragraph. Consequently the expected value in (1) can be broken into two parts which will be evaluated separately.

$$H = \langle \exp[\chi(\bar{\rho}_1, \bar{p}_1) + \ldots + \chi(\bar{\rho}_{2n}, \bar{p}_{2n})] \rangle \langle \exp[i\phi(\bar{\rho}_1, \bar{p}_1) - i\phi(\bar{\rho}_2, \bar{p}_2) + \ldots + i\phi(\bar{\rho}_{2n-1}, \bar{p}_{2n-1}) - i\phi(\bar{\rho}_{2n}, \bar{p}_{2n})] \rangle \quad (2)$$

The first term can be expressed as[33-35]

$$\langle e^{X_1 + X_2 + \cdots X_{2n}} \rangle = \int \cdots \int d\underline{\alpha}\, P_{\underline{X}}(\underline{\alpha}) e^{\alpha_1 + \alpha_2 \cdots \alpha_{2n}}$$

$$= \frac{1}{(2\pi)^n \left[\text{Det } \underline{\lambda}_{\underline{X}}\right]^{1/2}} \int \cdots \int d\underline{\alpha} e^{\underline{t}^T \underline{\alpha} - \frac{1}{2} (\underline{\alpha} - \overline{\underline{X}})^T \underline{\lambda}_{\underline{X}}^{-1} (\underline{\alpha} - \overline{\underline{X}})}$$

$$= e^{\underline{t}^T \overline{\underline{X}} + \frac{1}{2} \underline{t}^T \underline{\lambda}_{\underline{X}} \underline{t}} = e^{-2n\sigma_X^2 + \frac{1}{2} \sum_{j=1}^{2n} \sum_{i=1}^{2n} \lambda_{X_{ij}}} \tag{3}$$

where

$$\underline{\alpha} = \begin{bmatrix} \alpha_1 \\ \alpha_2 \\ \cdot \\ \cdot \\ \cdot \\ \cdot \\ \alpha_{2n} \end{bmatrix}$$

$$\underline{t} = \begin{bmatrix} 1 \\ 1 \\ \cdot \\ \cdot \\ \cdot \\ \cdot \\ \cdot \\ 1 \end{bmatrix}$$

$$x_j = x(\bar{\rho}_j, \bar{p}_j)$$

$$\underline{\bar{X}} = \begin{bmatrix} \langle x_1 \rangle \\ \cdot \\ \cdot \\ \cdot \\ \cdot \\ \langle x_{2n} \rangle \end{bmatrix}$$

$\underline{\lambda}_\chi$ is the covariance matrix for the log-amplitude, the underbars denote matrices and T indicates the transpose. The second expected value in (2) is given by

$$\langle e^{i\phi_1 - i\phi_2 \cdots - i\phi_{2n}} \rangle = \int \cdots \int e^{\underline{q}^T \underline{\alpha} - \frac{1}{2} \underline{\alpha}^T \underline{\lambda}_\phi^{-1} \underline{\alpha}} d\underline{\alpha}$$

$$= e^{\frac{1}{2} \underline{q}^T \underline{\lambda}_\phi \underline{q}} = e^{-\frac{1}{2} \sum_{j=1}^{2n} \sum_{i=1}^{2n} [-1]^{i+j} \lambda_{\phi_{ij}}} \tag{4}$$

where

$$\underline{q} = \begin{bmatrix} i \\ -i \\ \cdot \\ \cdot \\ \cdot \\ \cdot \\ \cdot \\ -i \end{bmatrix}$$

and $\underline{\lambda}_\phi$ is the covariance matrix for the phase perturbation term.

Equations (3) and (4) can now be combined to form the mutual coherence function. However, first we will express (3) in terms of the log-amplitude structure function $D_{\chi_{ij}}$ and covariance function $C_{\chi_{ij}}$ and will express (4) in terms of the phase structure function $D_{\phi_{ij}}$ where

$$D_{\chi_{ij}} = \langle[\chi(\bar{\rho}_i, \bar{p}_i) - \chi(\bar{\rho}_j, \bar{p}_j)]^2\rangle = 2\left(\sigma_\chi^2 - \lambda_{\chi_{ij}}\right)$$

$$D_{\phi_{ij}} = \langle[\phi(\bar{\rho}_i, \bar{p}_i) - \phi(\bar{\rho}_j, \bar{p}_j)]^2\rangle = 2\left(\sigma_\phi^2 - \lambda_{\phi_{ij}}\right).$$

and

$$C_{\chi_{ij}} = \langle[\chi(\bar{\rho}_i, \bar{p}_i) - \langle\chi\rangle]\,[\chi(\bar{\rho}_j, \bar{p}_j) - \langle\chi\rangle]\rangle$$

Equation (4) can then be rewritten as

$$e^{-\frac{1}{2}\left[\sum_{j=1}^{2n}\sum_{i=1}^{2n}[-1]^{i+j}\sigma_\phi^2 + \sum_{j=1}^{2n}\sum_{i=1}^{2n}[-1]^{i+j}\left[\lambda_{\phi_{ij}} - \sigma_\phi^2\right]\right]}$$

$$+\frac{1}{2}\sum_{j=i+1}^{2n}\sum_{i=1}^{2n-1}(-1)^{i+j}D_{\phi_{ij}}$$

$$= e^{-2n\sigma_\chi^2 - \frac{1}{2}\sum_{j=1}^{2n}\sum_{i=1}^{2n}(-1)^{i+j}\left[\lambda_{\chi_{ij}} - \sigma_\chi^2\right]} \qquad (5)$$

and equation (3) as

$$+\frac{1}{2}\sum_{j=1}^{2n}\sum_{i=1}^{2n}\left[1+(-1)^{i+j}\right]\lambda_{\chi_{ij}}$$

$$\frac{1}{2}\sum_{j=i+1}^{2n}\sum_{i=1}^{2n-1}(-1)^{i+j}D_{\chi_{ij}}+\sum_{j=i+1}^{2n}\sum_{i=1}^{2n-1}\left[1+(-1)^{i+j}\right]C_{\chi_{ij}}$$

$$=e \tag{6}$$

Using (5) and (6) in (2) the generalized mutual coherence function becomes

$$H=e^{\frac{1}{2}\sum_{j=i+1}^{2n}\sum_{i=1}^{2n-1}(-1)^{i+j}D_{\psi_{ij}}+\sum_{j=i+1}^{2n}\sum_{i=1}^{2n-1}\left[1+(-1)^{i+j}\right]C_{\chi_{ij}}} \tag{7}$$

where

$$D_{\psi_{ij}}=D_{\chi_{ij}}+D_{\phi_{ij}}$$

The two source wave structure function and the two source log-amplitude covariance functions are given by[19,7]

$$D_{\psi_{ij}}(\bar{\rho}_i,\bar{p}_i;\bar{\rho}_j,\bar{p}_j)=2.91\,C_n^2\,zk^2\int_0^1\left|t(\bar{p}_j-\bar{p}_i)+(1-t)(\bar{\rho}_j-\bar{\rho}_i)\right|^{5/3}dt \tag{8}$$

$$C_\chi(\bar{\rho}_i,\bar{p}_i;\bar{\rho}_j,\bar{p}_j)=0.132\,\pi^2k^2\int_0^L ds\,C_n^2(s)\cdot\int_0^\infty du\,u^{-8/3}\sin^2\left[\frac{u^2s(L-s)}{2kL}\right]J_o\left[u\left|(\bar{p}_j-\bar{p}_i)\frac{s}{L}+(\bar{\rho}_j-\bar{\rho}_i)\left(1-\frac{s}{L}\right)\right|\right] \tag{9}$$

It should be noted that (8) is in general good to second order in n_1 and for the case where ψ is jointly normal it is exact to all orders.[19] Equation (9) is good only to first order in n_1.[7]

Special cases are evaluated below for comparison with previously published results:

n = 1

$$H(\bar{\rho}_1, \bar{\rho}_2; \bar{p}_1, \bar{p}_2) = e^{-\frac{1}{2} D_{\psi_{12}}}$$

This is a well known result.[36-38]

n = 2

$$H(\bar{\rho}_1, \bar{\rho}_2, \bar{\rho}_3, \bar{\rho}_4; \bar{p}_1, \bar{p}_2, \bar{p}_3, \bar{p}_4) = \exp\left[-\frac{1}{2}(D_{12} - D_{13} + D_{14} + D_{23} - D_{24} + D_{34}) + 2C_{\chi_{13}} + 2C_{\chi_{24}}\right]$$

This is a generalization (double arguments) of the result of Ref. 39.

Although the above formulation for the generalized spherical wave mutual coherence function is strictly valid only when ψ is normally distributed, this is not an overly restrictive requirement. From physical reasoning and theoretical considerations, it can be shown that both the log amplitude and the phase are normally distributed to first order in n_1.[29,40] This has been confirmed by experiment.[41-49] Also, there is experimental evidence to suggest that χ is also normally distributed or nearly so for situations of practical importance under conditions of multiple scattering.[29,40-47] Since the larger scale sizes are more important with respect to phase effects, it seems reasonable that multiple scattering should be less important

and that the first order theory for phase effects should be valid even when the log-amplitude fluctuations are highly saturated. Measurements[48,49] of angle of arrival fluctuations tend to confirm this conclusion and it is generally believed that ϕ is indeed normally distributed with $\langle\phi\rangle = 0$.[29,40] Consequently, (7) should be valid in general for appropriate ranges of log-amplitude variance[29,40] and valid without restriction in special cases such as a large Fresnel number transmitter where the phase term is dominant.[50]